

**Estimation of Regional Net Surface Fluxes of CO₂ and O₃ Over Amazonia
from Aircraft Data**

A Thesis Presented by

Wendy Chou

to the Committee on Degrees in Environmental Science and Public Policy
in Partial Fulfillment of the Requirements for the Degree of Bachelor of Arts

Harvard University
Cambridge, Massachusetts

March 25, 1999

Acknowledgements

My deepest appreciation goes to my adviser, Steve Wofsy, for giving me sharper focus, profound insights, and much-needed programming guidance over the entire duration of this project. He showed by example that the questions raised in research might not always be answered, and instead continually lead to new challenges. I would like to recognize the immense contributions I received from John Lin, who bore the brunt of my questions and constantly supplied me with useful information and advice. Thanks also go to Brian Fehlau for attentive editing and Scott Saleska and Christoph Gerbig for substantive comments and suggestions. The entire Wofsy group (too many to name here) deserves my utmost gratitude for valuable feedback and encouragement.

ABSTRACT

Evidence suggests the existence of a 1-2 Gt so-called “missing” sink of atmospheric CO₂ in the terrestrial biosphere, but the distribution of this sink among the world’s ecosystems is still unknown. Tropical forests, of which the Amazon Basin represents the single largest area, account for 30-50% of terrestrial productivity and are potentially significant sinks in the global carbon cycle. Simultaneous measurements of CO₂, O₃, and CO concentrations from 14 flight missions in the lower troposphere over the Brazilian Amazon during the wet season (ABLE 2B Experiment, April-May 1987) were analyzed in order to estimate regional net surface fluxes of CO₂ and O₃. We used a “steady-state” approximation in which flux due to net biotic exchange was balanced by subsidence. Determination of the subsidence flux was accomplished by calculating the concentration gradient between the PBL and free troposphere and by using a mean subsidence rate of -600 m/day from NCEP analyzed fields for the experimental period. A linear decrease in CO₂ column amount over the day was observed and associated with a net CO₂ flux of -4.8×10^{12} molecules/cm²-s, representing a carbon sink of -0.84 kg C/ha-day. The CO₂ flux represents a weak net exchange corresponding to only -0.15 Gt C/y if projected to the whole basin. The results for O₃ showed a flux of -6.9×10^{10} molecules/cm²-s, consistent with other measurements from ABLE 2B. Our study indicates that regional net fluxes can be accurately determined using intensive airborne measurements and suggests attention to two issues of experimental design: (1) removal of anthropogenic combustion effects via a tracer (CO) can significantly affect the CO₂ flux estimate, and (2) flight data should be coupled with surface measurements between 0-150 m to fully account for behavior below the minimum altitude of the aircraft.

Table of Contents

Acknowledgements	1
ABSTRACT	2
Table of Contents	3
List of Figures	5
List of Tables	5
List of Abbreviations	5
Chapter 1: Motivations and Objectives	6
1. Motivations	7
1.1 Unresolved Issues of the Global Carbon Budget	7
1.2 Ozone Deposition	9
2. Processes which Affect PBL Concentrations of CO ₂ and O ₃	10
2.1 PBL Dynamics	11
2.2 Processes Affecting CO ₂ Concentrations	12
Photosynthesis and Respiration	12
Diurnal Rectifier Effect	12
CO Oxidation	12
2.3 Processes Affecting O ₃ Concentrations	13
Deposition of O ₃ to Canopy.	13
Photochemical Production and Chemical Loss of O ₃	14
3. Current Efforts to Estimate Fluxes	14
3.1 Diurnal Rectifier Effect	15
4. Analysis Objectives	15
Chapter 2: Data Source	18
1. ABLE 2B Description and Goals	18
2. Aircraft Data from ABLE 2B	20
2.1 ABLE 2B Aircraft Missions	20
2.2 Relevant Airborne Measurements: CO ₂ , O ₃ , CO	20
CO ₂ data	20
O ₃ data	21
CO data	22
3. Relevant In-Situ Surface Measurements: CO ₂ , O ₃	22
Chapter 3: Methods	25
1. Estimating Flux from Mean Column Concentration	25
2. PBL Variation and 24-Hour Averaging	26
3. Linear Model to Predict PBL Concentrations (Model 1)	26
3.1 Linear Model with Flight Factors (Model 2)	28
3.2 Selection of h and \bar{W}	28
3.3 Comparison of Predicted and Raw Data	29
Chapter 4: Results	41
1. Observed Concentration Profiles	41
2. Diurnal Trends in Aggregated Flight Data	41
3. Estimates of CO ₂ and O ₃ Gradients and Fluxes	42
3.1 Column Integral Method (Method A)	42
Effect of Flight Factors	43
Effect of Varying \bar{W}	43
3.2 Flux Inference by Similarity (Method B)	43
Chapter 5: Discussion	55
1. Sources of Error	55
1.1 Biases in the Data Source	55
1.2 Statistical and Systematic Error in the Data Analysis	56
1.3 Factors Affecting $\langle \bar{q} - q_h \rangle$ Gradient Estimation	56
Statistical Error	57

Error from \overline{W} Estimation	58
2. Extrapolation of Results to the Basin Scale	58
2.1 Summary of Other Estimates From the Field	58
Eddy Flux Towers	58
Eddy Correlation Onboard Aircraft	59
2.2 Spatial and Temporal Variability	60
Importance of Vegetation Type	60
Importance of Interannual Climate Variability	60
3. Implications for Future Experiment Improvement	61
Lower Boundary Conditions	61
Combustion and CO Oxidation	61
4. Conclusions	61
References	64
Appendix	68

List of Figures

Figure 1. Schematic of Diurnal Pattern of PBL Growth.....	17
Figure 2. Observed Response of NEE to PAR	17
Figure 3. Map of ABLE 2B Study Region	23
Figure 4. Seasonal Patterns of Rainfall and Water Level in the Amazon Basin.....	23
Figure 5. ABLE 2B Flight Study Area	24
Figure 6. Two Schematics of Diurnal Variation in CO ₂ Mean Column Concentration.....	30
Figure 7. CO ₂ Diurnal Concentration Variation Within PBL Contrasted to PBL Top.....	34
Figures 8a-f. Comparison of Raw Data to Predicted Data, Models 1 (Blue) and 2 (Pink).....	35
Figure 9. Hourly Plots of CO ₂ Observed Profiles	45
Figure 10. Hourly Plots of CO ₂ Observed Profiles.....	46
Figure 11. Hourly Plots of O ₃ Observed Profiles.....	47
Figure 12. Hourly Plots of O ₃ Observed Profiles.....	48
Figure 13. Vertical Profiles of Predicted CO ₂ From Aggregated Flight Data	49
Figure 14. Vertical Profiles of Predicted O ₃ From Aggregated Flight Data.....	50
Figure 15. Diurnal Trends in Mean Column Concentration: CO ₂ (upper plot) and O ₃ (lower plot)	51
Figure 16. CO ₂ Gradient $\langle \overline{q} - q_h \rangle$ for Predicted Data, Combustion Removed.....	52
Figure 17. O ₃ Gradient $\langle \overline{q} - q_h \rangle$ for Predicted Data, Combustion Removed	53
Figure 18. Dependence of CO ₂ Flux on \overline{W}	53

List of Tables

Table 1. Electra Aircraft Missions During ABLE 2B	24
Table 2. Regression Statistics for CO ₂ Linear Model 1	31
Table 3. Regression Statistics for O ₃ Linear Model 1	32
Table 4. Comparison of r ² Values: CO ₂ Model 1 vs. CO ₂ Model 2 (Added Flight Factors).....	33
Table 5. Comparison of r ² Values: O ₃ Model 1 vs. O ₃ Model 2 (Added Flight Factors).....	33
Table 6. Diurnal Variation of Boundary Layer Height.....	34
Table 7. CO ₂ Daytime Gradients $(\overline{q} - q_h)$	52
Table 8. O ₃ Daytime Gradients $(\overline{q} - q_h)$	52
Table 9. Summarized Flux Estimates: CO ₂ and O ₃	54
Table 10. CO ₂ Flux Estimation by Similarity.....	54
Table 11. Table showing sample sizes used in the column integral procedure.	63

List of Abbreviations

ABLE	Amazon Boundary Layer Experiment
CBL	Convective Boundary Layer
CMDL	Climate Monitoring and Diagnostics Laboratory
DIAL	Differential Absorption Lidar
GCM	General Circulation Model
GMDF	Global Meteorological Data Facility
GMT	Greenwich Mean Time
GOES	Geosynchronous Operational Environmental Satellite
GPP	Gross Primary Productivity
Gt C	Gigaton of Carbon = 10^{15} g C
GTE	Global Tropospheric Experiment
ha	Hectare = 10^4 m ²
IRI	International Research Institute
INPA	Instituto de Pesquisas da Amazonia
INPE	Instituto de Pesquisas Espaciais
IPCC	Intergovernmental Panel on Climate Change
LaRC	Langley Research Center
LDEO	Lamont-Doherty Earth Observatory
LT	Local Time
NASA	National Aeronautics and Space Administration
NCAR	National Center for Atmospheric Research
NCEP	National Centers for Environmental Prediction
NEE	Net Ecosystem Exchange
NEP	Net Ecosystem Productivity
NOAA	National Ocean and Atmosphere Administration
NPP	Net Primary Productivity
PAM	Portable Automated Mesonet
PAR	Photosynthetically Active Radiation
PBL	Planetary Boundary Layer
ppb	parts per billion
ppm	parts per million
ppt	parts per trillion

Chapter 1: Motivations and Objectives

Atmospheric science has focused increasingly on issues of human interaction with our environment, addressing how we may be altering its state, as well as how changes in the environment may affect our lives. Tropical forests constitute a major ecosystem type whose interaction with the atmosphere has global import, yet a scarcity of comprehensive data on these areas has been a major obstacle until recent decades. This analysis focuses on data acquired over the Amazon rain forest, the principal tropical forest in South America and the world's largest area of undisturbed forest. The Amazon Basin spans about 6 million square kilometers, covering 30% of the land area in the equatorial belt and comprising an estimated 39% of the world's total rain forest area (Santos 1987).

Carbon dioxide (CO₂) and ozone (O₃) are trace gases of growing importance with respect to tropical forest processes and productivity. The rise in atmospheric CO₂ concentrations during the past century due to anthropogenic combustion has fueled serious concerns over potential climate change and global warming. Thus, one of the most important challenges for atmospheric research today is to evaluate the consequences of increasing CO₂ emissions on the global carbon cycle, an issue of great uncertainty. The known CO₂ emissions rate is incompatible with current observations of atmospheric concentrations of CO₂, with the latest studies showing the probability of a "missing sink" of CO₂ in the terrestrial biosphere. Due to its large area, tropical forest may account for a meaningful fraction of this sink. Quantifying carbon uptake by tropical forests, however, is an ongoing matter of debate impeded by a deficiency of actual field measurements.

Tropospheric ozone (O₃) is another topic of interest in the tropics, a region where rapid photochemistry takes place. The deposition of O₃ to tropical vegetation may be a significant sink in the global cycle of this reactive gas, and its effect on the health of tropical canopies, not yet carefully assessed, may grow if O₃ concentrations continue to rise in remote regions. In addition, the measurement of the surface flux of O₃ provides another technique of appraisal for the surface fluxes of CO₂, because CO₂ fluxes may be inferred by similarity arguments from knowledge about O₃ deposition.

1. Motivations

1.1 Unresolved Issues of the Global Carbon Budget

Intense controversy has surfaced in the global scientific community over the fate of CO₂ emitted as a result of fossil fuel burning. The anthropogenic emission rate of CO₂ is currently estimated about 6-7 Gt C per year (Gt=10¹⁵ g) (Prentice and Lloyd 1998) roughly double the actual growth rate in the observed global concentration of atmospheric CO₂, about 3-4 Gt per year (IPCC 1994). Thus, the central question is simple: where does the rest of the carbon go? With an estimated 10% accuracy, the anthropogenic fossil fuel contribution is the most quantifiable flux in the global carbon cycle; relatively speaking, other CO₂ source processes such as conversion of CO to CO₂, tropical deforestation, and outgassing from oceans are less well-defined (Anderson *et al.* 1996). But harder still is determining the distribution of the “missing” 2-3 Gt C as it is taken up by both the terrestrial biosphere and the oceans. Thus, a balanced carbon budget which accurately quantifies both sources and sinks remains an elusive goal for atmospheric scientists.

At the beginning of this decade, atmospheric modelers proposed a global carbon budget which included a greater northern hemisphere sink for CO₂ than had been previously assumed; furthermore, this sink was hypothesized to be terrestrial. Evidence in these early studies that northern hemisphere terrestrial uptake might explain much of the “missing sink” rested in observations of a north-south interhemispheric atmospheric CO₂ gradient that was smaller than atmospheric transport models had projected to arise from the dominance of northern hemispheric industrial sources. For instance, Tans *et al.* (1990) calculated a theoretical meridional gradient of about 6-7 ppm over the period 1980 to 1987, while actual observations showed only a ~3 ppm pole-to-pole difference during those years. Their empirical judgment of the global atmosphere-ocean flux was -1.6 Gt C (out of the atmosphere). Therefore, Tans *et al.* (1990) inferred a northern hemisphere terrestrial sink of 2-3 Gt C per year to account for the remaining uptake.

Several newer studies have emerged which support the northern hemisphere sink theory. For instance, Fan *et al.* (1998) used improved and expanded modeling

schemes and an inverse analysis. They concluded that, while atmospheric CO₂ saw a 2.8 Gt C per year increase during the period 1988-1992, the Northern hemisphere terrestrial biosphere took up 1.7 (\pm 0.5) Gt C per year during that time (including 1.4 \pm 0.4 Gt C per year in North America), decreasing the north-south gradient from 4-5 ppm to 3 ppm (Fan *et al.* 1998). A sink of 3.5 Gt in Northern hemisphere between 30°N and 60°N was proposed by a group of scientists using ¹³C/¹²C measurement techniques (Ciais *et al.* 1995). Many other atmospheric modelers have supported the northern hemisphere sink hypothesis with varying estimates of its magnitude (Conway *et al.* 1994; Denning *et al.* 1995).

Other recent studies have agreed upon the terrestrial biosphere as the locus of the missing sink, but have argued that significant uptake is occurring in the tropics in addition to temperate latitudes (Grace *et al.* 1996b; Phillips *et al.* 1998). Because the Amazon rain forest (with an estimated area of 6 x 10⁶ km²) is a major subset of tropical forest, and a major global reservoir for organic matter (about 20% of global forest carbon) this ecosystem has received much attention. Using eddy correlation techniques in Rondônia, Brazil (10°S, 57°W), Grace *et al.* observed net uptake of CO₂ that, when extrapolated for the entire Basin, accounted for a sink of ~0.5 Gt C per year. They derived this annual value from continuous eddy flux measurements which lasted for periods of four to six weeks during both summer and winter seasons (Grace *et al.* 1996b).

Direct measurement of biomass in forests offers an alternative to the indirect estimate of uptake through atmospheric modeling. One recent study measured the change in biomass in ecological plots in mature tropical rain forests in South America, concluding that an estimated 0.7 (\pm 0.34) tons C per hectare per year were accumulated by these forests (Phillips *et al.* 1998). This figure represents a sizeable ~40% of the missing sink of ~1.4 Gt per year as estimated by Schimel (1995). If the biomass argument is plausible in the tropics, it would appear to be very significant. By contrast, forest inventories in the temperate zones have not kept pace with the sink estimates suggested by the atmospheric models. Brown and Schroeder (1999, in press), for instance, determined that forest uptake in 28 eastern U.S. states over the late 1980s-early 1990s was only 0.17 Gt C per year. One explanation for this

disparity is that North American forests are not taking up as much carbon as the atmospheric models purport. However, the “bottom-up” approach of direct biomass measurement does have uncertainties. For example, U.S. forest inventories have been primarily aboveground, while estimates of below-ground carbon (i.e. roots) have not yet been carefully verified (Brown *et al.* 1997; Schroeder *et al.* 1997). Furthermore, the relationship between carbon uptake and production of new biomass is complicated by processes such as oxidation of soil organic matter. In addition, some suggest that volatile hydrocarbons emitted by plants represent an important additional pathway by which carbon is released to the atmosphere, rather than assimilated as new biomass (Fan *et al.* 1998). All these concerns may be relevant for forest inventories in the Amazon as well in the Northern Hemisphere.

As the existing literature shows, the scientific community has not yet reached a consensus over the global distribution of the missing carbon sink, including the amount of uptake attributed to tropical forests. The context of the global carbon budget controversy necessitates better assessments of the magnitude of the tropical forest carbon sink. The primary goal of our analysis is thus to derive a rough estimate of the surface CO₂ flux over Amazonia.

1.2 Ozone Deposition

The current significance of the Amazon rain forest for scientists extends well beyond the uncertainties of CO₂ uptake. One topic of great atmospheric and ecological significance is the interaction of O₃ with tropical forest canopies. The exchange of O₃ between atmosphere and biosphere is especially rapid in tropical environments, where abundant sunlight and high temperatures and humidity speed reaction rates (Fan *et al.* 1990). The sheer expanse of the Amazon rain forest, an estimated 39% of the world’s total rain forest area (Santos 1987) suggests that, because deposition of ozone to tropical forests represents an important sink in the global cycle of O₃, the proportion of this deposition occurring in the Amazon itself is perhaps significant in the total ozone budget (Fan *et al.* 1990).

The effect of O₃ pollution on tropical vegetation is an area of concern for plant biologists and ecologists. This effect has not yet been rigorously studied for tropical

ecosystems, partly because of the difficulties in accessing these remote areas, and partly because concentrations of O_3 in these regions are relatively low. However, the observed increase in global tropospheric concentrations may be cause for increased study of the toxicity of O_3 to tropical vegetation.

The above statements provide the rationale for O_3 to be studied as an independent species. However, calculation or measurement of O_3 fluxes may serve the added purpose of better quantifying carbon fluxes. If information is known regarding the concentrations of O_3 and CO_2 both within and above the planetary boundary layer (PBL), and the surface O_3 flux can be quantified, one can draw inferences of CO_2 flux by similarity. Before delving further into these more mathematical principles, however, it may be useful to review the basic dynamical, biological, and chemical processes which take place within the PBL.

2. Processes which Affect PBL Concentrations of CO_2 and O_3

The concentration profile of a trace gas such as CO_2 or O_3 varies over the course of the day due to physical, biological, and chemical forcings. Using the concepts of the simple box model and mass balance, one can enumerate several factors which cause changes in the amount of CO_2 or O_3 in the box, such as transport into and out of the box, and chemical production and loss. We will refer to the ensemble of factors which determine PBL concentrations of a particular species as its *PBL budget*. For CO_2 the major factors include: (1) PBL dynamics such as entrainment flux and mean subsidence; (2) photosynthesis and respiration in the forest canopy and soils); and to a lesser extent, (3) combustion. An additional term which is critical to understanding variations of CO_2 in the PBL is the *diurnal rectifier effect*, which arises due to correlation between factors (1) and (2) above. For O_3 , the factors are: (1) PBL dynamics; (2) deposition to forest canopy when stomata are open; and (3) photochemical production and chemical loss. For both gases, this study assumed negligible effects from horizontal advection.

2.1 PBL Dynamics

The planetary boundary layer (PBL) is the lowest layer of the troposphere and represents the region most strongly influenced by conditions at the earth's surface. For example, the convection of air parcels within the PBL is caused by turbulence driven by solar radiation influx. Heat, momentum, and water and other trace gases are generally well-mixed in the PBL due to convection. Over land, the height of the PBL extends from 100 m (at night) to about 3000 m (at noon), growing and decaying in response to changes in turbulent convection. This phenomenon is quite weak over the ocean due to the greater heat capacity of water. On land, however, the diurnal fair-weather pattern of the boundary layer growth has important consequences for both CO₂ and O₃ in the PBL. (Stull 1988)

Before sunrise, the absence of radiatively-driven convection is associated with a low boundary layer height, implying a small mixing volume within the PBL. As solar radiation increases during a sunny day, the region in the PBL which undergoes mixing grows as less turbulent air from above becomes *entrained* by mixing into the PBL. PBL growth over the day is illustrated in Figure 1. A typical entrainment velocity is about 0.01 to 0.20 m/s (Stull 1988). If air parcels above the PBL have a different concentration than those within the PBL, entrainment flux will cause changes in PBL concentration.

The PBL is also permeable to vertical flux due to *subsidence* (We will designate this term as W with the understanding that negative W indicates downward movement). Field experiments have observed that the mean vertical velocity ranges from about -0.22 m/s to +0.27 m/s (Vachalek *et al.* 1988). Again, any gradient between the concentrations above the PBL and the concentrations within the PBL will cause a change in PBL concentration as the air from aloft mixes across the boundary into the PBL.

The physical dynamics of the PBL are similar for both CO₂ and O₃. However, discussion of additional biological and chemical factors requires us to differentiate between these gases.

2.2 Processes Affecting CO₂ Concentrations

Photosynthesis and Respiration

Photosynthesis, the uptake of CO₂ by plants to form carbohydrates, and respiration, the release of CO₂ following oxidation of these compounds for energy, are the dominant natural processes capable of rapidly affecting the transfer of carbon between the biosphere and the atmosphere. Thus the exchange of CO₂ between the biosphere and the atmosphere in forests represents a critical part of the global flux of carbon on a short time scale.

The functional relationship between photosynthesis and photosynthetically active radiation (PAR) has been well documented, while respiration occurs both in the presence and absence of PAR. Net ecosystem exchange (NEE), the net transfer of carbon from the entire ecosystem to the atmosphere (i.e., negative NEE indicates uptake) due to photosynthetic and respiratory processes, has been shown to experience well-defined diurnal variations which are dictated by the availability of solar radiation (Fan *et al.* 1990; Grace *et al.* 1995) (Figure 2). The temporal aspect of CO₂ exchange between the biosphere and atmosphere is critical to understanding CO₂ concentration variations in the PBL.

Diurnal Rectifier Effect

The time scale of PBL growth and decay covaries with that of plant photosynthesis and respiration, resulting in a phenomenon called the “diurnal rectifier effect” This rectifier involves contrasting situations for daytime and nighttime CO₂ concentrations. A seasonal rectifier differentiating summer conditions from winter conditions also exists, but is not addressed in this analysis. In essence, the strongest turbulent mixing, associated with PBL growth during the day, occurs when net photosynthetic uptake is also strongest. At night, the mixing volume is shallow as the canopy respire, resulting in high CO₂ concentrations. The diurnal rectifier is discussed at greater length in Section 3.1 of this chapter.

CO Oxidation

The conversion of CO into CO₂ ($\text{CO} + \text{OH} \rightarrow \text{CO}_2 + \text{H}$) is a chemical process dependent on the presence of the OH radical, which is relatively more abundant in the

tropics due to the higher availability of solar radiation. However, because the Amazon sees little advected pollution (other than from Manaus) the local sources of CO are small. In the total CO₂ budget of the PBL, oxidation of CO is a much smaller factor than photosynthesis or rectification.

2.3 Processes Affecting O₃ Concentrations

As summarized in Jacob and Wofsy (1990), the O₃ budget includes effects from biosphere-atmosphere exchange, photochemistry, vertical mixing, and long-range transport of pollutants. Two very significant processes which affect O₃ concentrations are: deposition to the canopy, and net chemical production (P+L) determined by both photolysis as well as the chemistry of NO_x. In the Amazon, low NO_x results in a relatively greater effect due to deposition.

Deposition of O₃ to Canopy.

An important O₃ sink is dry surface deposition, which includes significant deposition to vegetation and thus to forest canopies. This flux is typically defined as $F=[O_3](z) \times V_d$ where the proportionality constant, V_d , is the deposition velocity. Deposition velocity, ranging from 0-1 cm/s in temperate forest (Munger *et al.* 1996), has an observed diurnal pattern that peaks at midday (Fan *et al.* 1990) and depends primarily on stomatal conductance, as well as on complex micrometeorological transfer processes such as wind direction, air temperature, solar radiation, and chemical processes above and within the forest canopy (Munger *et al.* 1996; Sandermann *et al.* 1997). Because deposition to the canopy occurs when the stomata on the leaves are open, it occurs to a much smaller degree at night.

The influence of photosynthesis on the CO₂ budget represents a close link between the CO₂ budget and the forest canopy; similarly, the depositional flux of O₃ is a crucial biotic factor in the O₃ budget. However, O₃ concentrations are also influenced to a greater degree by additional complex photochemical production and loss processes than are CO₂ concentrations.

Photochemical Production and Chemical Loss of O₃

Photochemical production occurs with much greater frequency in the stratosphere, where photons are more abundant. Transport of photochemically produced O₃ from the stratosphere into the free troposphere is a significant source in the PBL due to its subsequent entrainment.

O₃ is cycled as a result of chain reactions involving NO_x (NO + NO₂), HO_x (OH and HO₂) and CO in the presence of light. The main source of NO_x is anthropogenic combustion (accounting for nearly 50% of global sources), while primary hydrocarbon and CO sources include fossil fuel combustion and oxidation of methane and other trace hydrocarbons. However, O₃ is also related to presence of NO_x from soils produced from microbial activity, which drives chemical loss of O₃. Thus, the amount of atmospheric NO influences concentrations of O₃ by controlling chemical production and loss .

O₃ mechanisms are known to depend heavily on NO_x levels. Studies have shown that the pristine atmosphere of the Amazon during the wet season generally does not support O₃ production due to low NO (Jacob and Wofsy 1990). Modeling results from Jacob and Wofsy (1990) showed that during the day, the effect of deposition on the concentration of O₃ (-9000 ppt/h) far outweighed the net effect of chemical production and loss (+150 ppt/h) (Jacob and Wofsy 1990) The conclusion of Jacob and Wofsy (1990) was that concentrations of O₃ in the PBL show a balance between supply from the free troposphere and removal by deposition to vegetation.

3. Current Efforts to Estimate Fluxes

Several techniques exist for estimating the magnitudes of regional trace gas fluxes, including CO₂. These include direct measurement at eddy flux towers (Fan *et al.* 1990; Grace *et al.* 1995; Grace *et al.* 1996a; Grace *et al.* 1996b; Wofsy *et al.* 1988) as well as inferred estimates through biomass change (Turner *et al.* 1995, Phillips *et al.* 1998). Another approach is the so-called “inverse method,” or “inverse analysis,” which uses spatial variations in concentration data to estimate sources and sinks (Enting *et al.* 1995; Stephens *et al.* 1998). A variation known as the “CBL budget method” (in reference to the convective boundary layer, a synonym for the PBL)

(Denmead *et al.* 1996; Raupach *et al.* 1992) utilizes temporal variations in concentration data. A problem with both methods is that the global observational network for atmospheric CO₂ consists primarily of surface observations, which can bias calculations of flux by neglecting the diurnal rectifier effect.

3.1 Diurnal Rectifier Effect

A study by Denning *et al.* (1996) involved the coupling of a general circulation model (GCM) and a biosphere model to show that during the day, mixing and PBL growth occur simultaneously with photosynthetic uptake; by contrast, the shallow height of the nighttime PBL occurs during a period of respiration. During early morning, CO₂ concentrations near the surface contain the previous night's residual respired CO₂. Air further above sees much lower concentrations due to the effect of photosynthesis, which depletes CO₂, and the distribution of respired CO₂ over a much larger mixing volume due to PBL growth. As a result, the CO₂ profile is stratified, with lower altitudes having higher relatively average CO₂ concentrations and higher altitudes having relatively lower concentrations compared to a scenario without rectification. Overestimating surface concentrations may lead to an underestimation of the magnitudes of terrestrial sinks. Thus, after taking into account the rectifier effect, the interhemispheric gradient calculated at the surface by Denning *et al.* (1996) was nearly half as strong as the gradient assumed from fossil fuel emissions, implying a Northern Hemisphere sink larger by 1.2-2.5 Gt C/yr.

One way to resolve the bias at the surface caused by the diurnal rectifier is to sample a wider altitude range. This analysis was able to utilize data from multiple vertical profiles which better characterized the pattern of diurnal variation. As described in Chapter 2, these profiles extended, during some flights, beyond 4 km. The flights in total spanned a daytime period of roughly 0700-1700 local time (LT).

4. Analysis Objectives

The primary objective of this analysis was to estimate 24-hour average surface fluxes for CO₂ and O₃ for the Amazon region from existing data of CO₂ and O₃ daytime concentrations within and just above the PBL by assessing changes in mean

column concentrations. The data set chosen was a robust collection of daytime vertical concentration profiles from airborne measurements in the PBL above the Brazilian Amazon, taken during the Amazon Boundary Layer Experiment 2B campaign (April-May, 1987). As mentioned in the previous section, the advantage of vertical profiles is that they are less biased than measurements acquired solely at the surface.

Another advantage of studying both CO₂ and O₃ simultaneously was that the knowledge of one tracer flux could lead to the estimation of the other by similarity. In other words, knowledge of the rate of O₃ flux could be used to calculate the flux of CO₂, assuming that the tracers have similar transport characteristics. This “similarity method” provided a second means of estimating the flux.

A secondary objective of the analysis was to verify the degree to which results generated by this analysis could be corroborated with other available evidence. To the best of our knowledge, does this method of analysis provide numbers reasonable enough to warrant its further use? What were the limitations on its accuracy? One important method of verification of an aircraft-based analysis was to compare the obtained results to flux data from eddy correlation measurements on the ground, as well as flux estimates from other studies. Another component of the verification process was to identify possible areas of systematic or statistical bias in both the experimental design and the data analysis. Ideally, this knowledge could be used to avoid problems of bias in future studies of trace gas fluxes using similar methods.

In summary, the wealth of data provided by the ABLE 2B study offered an opportunity to investigate the viability of deriving CO₂ and O₃ flux estimates from a robust data set of PBL concentrations from intensive aircraft sampling.

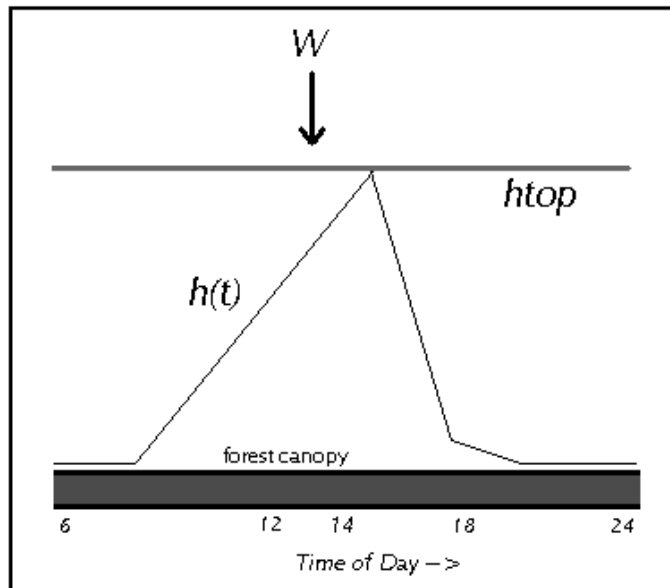


Figure 1. Schematic of Diurnal Pattern of PBL Growth

The PBL height grows to a maximum around 1400 and then collapses. Subsidence (W) at the top of the PBL is shown.

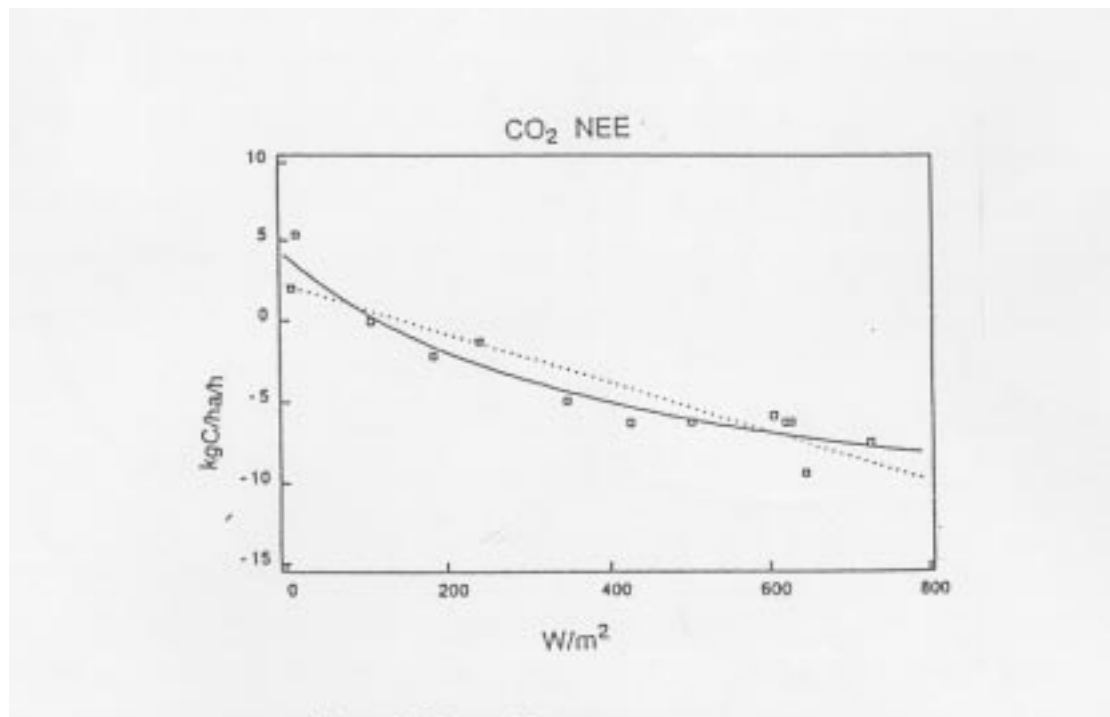


Figure 2. Observed Response of NEE to PAR

Source: Fan et al. (1990). Uptake is stronger with increasing solar flux.

Chapter 2: Data Source

1. ABLE 2B Description and Goals

The Amazon Boundary Layer Experiment 2B (ABLE 2B) was conducted in the Brazilian Amazon during April and May 1987, the sixth and seventh months of the 9-month wet season. The experiment is described more fully in Harriss *et al.* (1990). Its predecessor, ABLE 2A, took place in roughly the same region of Amazonia during the dry season months of July and August 1985 (Harriss *et al.* 1988). As part of NASA's long-term Global Tropospheric Experiment (GTE), both phases of ABLE 2 were designed to further our understanding of the chemistry and dynamics of the planetary boundary layer (PBL) over Amazonia by acquiring high resolution data on a variety of spatial scales (McNeal 1988). Due to its remote location and its comprehensive measurements, ABLE 2B was a unique experiment, representing the first in-depth study of regional scale PBL chemistry and dynamics over relatively undisturbed tropical forests and wetlands during the wet season.

The study took place in the central Amazon Basin as shown in Figure 3, stretching from Tabatinga in the west (70° W) to Belem in the east (49° W). Prior to ABLE 2B, little knowledge existed regarding wet season conditions in tropical rain forests, as studies more frequently occurred during the dry season for logistical reasons. However, since the dry season typically lasts only 3-4 months, estimates of annual behavior incorporating only dry season measurements are likely to be biased. Thus, the 8-9 month wet season deserves greater consideration when generalizing over an entire year. (Figure 4)

ABLE 2B drew together over 100 American and Brazilian scientists researching four primary areas: (1) spatial and temporal variability in trace gases (such as CH₄, CO, CO₂, NO, NO_y, and O₃) and aerosols; (2) the effect of atmospheric convection and other motion on distribution of chemical species; (3) exchange rates for trace gases between the biosphere and atmosphere using micrometeorological measurements; and (4) development of chemical and dynamical models for explaining observed distributions of trace gases (Harriss *et al.* 1990a). ABLE 2B was seminal in recording the first airborne ozone flux measurements obtained over a

tropical rain forest, as well as the first airborne measurements of CO (Ritter *et al.* 1990).

The synthesis of information from multiple spatial scales also distinguished ABLÉ 2B remarkably from earlier experiments. Data were collected at local, regional, and global scales, utilizing ground, aircraft, and satellite measurements. A tower 45 m in height, located at the Ducke Forest Reserve (60° W), ~20 km northeast of Manaus, was the focus for continuous surface measurement of chemical species and atmospheric dynamics. The specifics of the tower site eddy flux measurements have been discussed more comprehensively previously (Shuttleworth *et al.* 1984). Regional measurements also included daily rawinsondes soundings at approximate three-hour intervals and tethered balloon soundings. At the Ducke site, a tethered balloon was flown from the surface to 1200 m, while tethered balloons soundings at the EMBRAPA and Carapana stations were flown from 0 to 500 m. Geosynchronous Operational Environmental Satellite (GOES) imagery was available through resources at Langley Research Center (LaRC) for the purposes of study of mesoscale and synoptic-scale systems and convective activities. (Garstang *et al.* 1990) A more thorough descriptions of these measurements is presented in Harriss *et al.* (1990).

Most important for this analysis, a NASA Wallops Flight Center Electra aircraft equipped with instrumentation for measuring CO₂, O₃, CO, aerosols, and various dynamical parameters, flew 21 missions over the study region. The total flight study area covered a distance of approximately 1500 km from east to west, roughly following the path of the Amazon River. The flight study area was bounded on the east by the Atlantic Coast, including, at the southeast corner, an area surrounding the town of Belem, and spanned westward to the inland and more urban site of Manaus. (Harriss *et al.* 1990a) (Figure 5). The flight missions and the suite of measurements obtained from these missions are more fully detailed in the following section.

2. Aircraft Data from ABLE 2B

2.1 ABLE 2B Aircraft Missions

The 21 missions executed by the Electra aircraft were designed to achieve four distinct goals. Latitude “survey” missions were flights between Manaus and other cities such as Santarem (roughly halfway between Manaus and Belem). Cross-basin *survey* missions spanning Manaus to Belem investigated the distribution of trace gases and aerosols over the large scale. *Source* missions studied the chemistry of the lower troposphere over a particular environment type, such as forest or wetland, via repeated flights at varying altitudes over the designated area. Convective *transport* missions of three flight patterns (“volume”, “double volume”, and “single wall”) looked at the impact of clouds and mesoscale convective systems on the concentration distribution of trace gases and aerosols. The *flux* mission flight path resided predominantly through the PBL.

Of the 14 missions which constituted the focus of this analysis, five were source missions (one of which was wetlands rather than forest), three were transport missions (“volume” flight pattern) and one was a flux mission (Table 1). The altitude ceiling for the experiment was roughly 5 km, although the aircraft itself was capable of flying to about 9 km. The majority of the flights, however, took place between 0.15 and 3.1 km. All flights took place between 0700-1700 local time (GMT – 4 hours).

2.2 Relevant Airborne Measurements: CO₂, O₃, CO

Measurements of meteorological parameters, atmospheric concentrations of CO₂, O₃, CO, water vapor, sulfur, aerosols, methane, nitric oxide, PAN, isoprene, and radon took place onboard the NASA Electra aircraft. The measurements of most interest in this study were those of CO₂, O₃, and CO. Methods of data collection for these gases are encapsulated below.

CO₂ data

Carbon dioxide concentrations were measured using a BINOS non-dispersed infrared analyzer on the NASA Electra. Air was drawn through the apparatus by a downstream pump, after first being brought to a constant dew point by passing

through a wet trap maintained at 0° C, then passing through a pressure control solenoid valve and into the sample cell. Reference gas with approximately ambient concentration of CO₂ in dry air was passed through the reference cell. The pressure in both cells was maintained constant using an MKS capacitance manometer and pressure controller. Standard Reference Materials obtained from the national Bureau of Standards were used to calibrate the instrument in flight by replacing the air stream with the standards prior to passing through the wet trap. Concentrations in the standard bracketed the observed concentrations in the atmosphere and were stated to be accurate to ±2 ppm. Only one set of standards was used in the experiment, therefore long-term precision of the measurements approached the instrument resolution of ±0.1 ppm in level flight. (S.C. Wofsy, personal communication, 1999)

The BINOS instrument exhibited sensitivity to attitude and aircraft motion, apparently due to deflection of the infrared source. The deflection was reproducible and a first-order correction was made using data from a tri-axial linear accelerometer attached to the instrument. Data from the accelerometer obtained during calibration cycles were fit to a 2nd-order polynomial to obtain a correction factor, which was then applied to the ambient data. However, residual sensitivity to aircraft motion was apparent, due primarily to rotational accelerations during turbulence and during spiral turns made in vertical profiling. Thus, the resolution of the instrument in level flight was degraded to about ±0.5 ppm during the vertical profiles. This error was assumed to average out over the course of the experiment. (S.C. Wofsy, personal communication, 1999)

O₃ data

O₃ concentrations were measured by Gregory *et al.* (1990) using ethylene C₂H₄ chemiluminescence techniques, with data averaged either over 10 s or 1 minute (Gregory *et al.* 1990). Additional ozone measurements were acquired via an airborne Differential Absorption Lidar (DIAL) remote sensor with a vertical resolution of 15 m, and a C₂H₄ chemiluminescence system described in greater detail in Browell *et al.* (1990). As previously mentioned, the airborne measurements of O₃ flux during ABLE 2B were the first such measurements performed over a tropical rain forest biome.

These measurements were obtained via NO chemiluminescence methods with a 10-Hz response (Ritter *et al.* 1990).

CO data

Measurements were made using a Differential Absorption CO Measurement (DACOM) fast-response instrument sampled at a 10 s interval. Measurement precision was estimated $\pm 2\%$ (2σ) and measurement accuracy was estimated to be $\pm 4\%$ (2σ) (Harriss *et al.* 1990b).

3. Relevant In-Situ Surface Measurements: CO₂, O₃

The CO₂ and O₃ eddy correlation measurements at the Ducke tower represented the first such measurements taken over tropical forest (Fan *et al.* 1990). Measurements of CO₂ flux, O₃ flux, and vertical wind speed (w) were acquired 10 times per second and averaged with a Campbell Scientific Datalogger at 1-second intervals. CO₂ flux was measured with a BINOS non-dispersed IR analyzer, while O₃ flux was analyzed via C₂H₄ chemiluminescence. w was measured using a single-axis sonic anemometer (Campbell Scientific Inc.). Error in the flux measurements was determined to be of three types: (1) errors in the time delays of the Datalogger, (2) instrumental zero drift, and (3) aliasing of the high-frequency noise from the sensors. A time delay of 0.1 s was estimated to result in a 1% error for both CO₂ and O₃. Instrumental zero drift was estimated to be small; fluxes were determined to be consistent to better than 15% over most intervals. Fourier transform showed no significant contributions from frequencies above 1 Hz for CO₂ and O₃ (Fan *et al.* 1990).

Concentrations were measured for both gases at eight heights on the tower (0.02, 3, 6, 12, 27, 36, 41 m) (Fan *et al.* 1990), though only the 41 m measurements were used for this analysis. CO₂ was measured using a Beckman 865 non-dispersed infrared analyzer while O₃ was measured using a Dasibi 1003-AH ozone analyzer. The O₃ methods are more fully detailed in Bakwin *et al.* (1990).

Chapter 3: Methods

1. Estimating Flux from Mean Column Concentration

The conceptual basis for our methods begins with the mass continuity of a chemically inert species (such as CO₂) for which $P - L = 0$:

$$\frac{\partial n_q}{\partial t} + \nabla \cdot \Phi_q u = 0 \quad (3.1)$$

Eqn. 3.1 can be integrated over a column volume of unit area and fixed height h (m) which is just above the maximum height of the PBL, a derivation which is shown in Appendix I. The derivation calls upon the *mean column concentration* (\bar{q}) for a column of air with height h :

$$\bar{q} = \frac{\int_0^h q(z,t) dz}{h} \quad (3.2)$$

Here, q is concentration (ppm or ppb), n is air density (molecules/cm³), and z and t are altitude (m) and time (s), respectively. Like q , \bar{q} has units of ppm (for CO₂) or ppb (for O₃).

Next, we imagine a simple fair-weather model of PBL dynamics in which subsiding air (with mean vertical velocity \bar{W}) enters the column at h , bringing concentration $q_{z=h}$ (q_h) down into the column. This air must exit the column by the principle of continuity. The simplest explanation for how this is accomplished is via constant horizontal divergence out through the sides of the column. On average, this horizontal flow carries air of concentration \bar{q} . However, q_h and \bar{q} are not equal, so to satisfy continuity, the difference term must be the surface flux, S , the time-varying flux at the surface (in molecules/cm²-s). The value of \bar{q} (for the column below h) varies over time due to chemical and biological processes, but is not affected by growth of the PBL, because the PBL never extends to the height of h . The value of q_h , by contrast, has a negligible diurnal cycle as shown in Section 2.1 of this chapter.

Because photosynthesis and respiration affect the CO₂ concentrations in the column over the day, S is thus an estimate of net ecosystem exchange (NEE). A plot of mean column concentration versus time over a typical day has positive slope in the

evening, when respiration dominates, and negative slope during the daytime, when the rate of photosynthesis exceeds that of respiration. Though the exact shape of the function is unknown, it can be approximated either as a sinusoidal or a straight-line figure with a minimum at 1700 and a maximum at around 0700, as the schematics in Figure 6 show. Evidence for these times is derived from (1) the relationship of NEE to solar flux (see Chapter 1, Fig. 2) and (2) the diurnal variation of solar flux. The ABLE 2B aircraft data provided a daytime range (0700-1700) of concentration data from which hourly mean column integrals were derived. We hypothesized that this time range captured the turning points of the mean column concentration curve.

2. PBL Variation and 24-Hour Averaging

Averaged over a 24-hour period (signified by $\langle \rangle$), $\langle \bar{q} \rangle$ is assumed to remain in steady state. The surface sink or source term, time-averaged over 24 hours, is then:

$$\langle \bar{q} - q_h \rangle = - \frac{\langle S \rangle}{\langle \bar{W}_h \rangle n_h} \quad (3.3)$$

For our analysis, solving for $\langle S \rangle$ involved: (1) the calculation of \bar{q} at hourly timepoints by integrating concentration profiles to h , (2) the determination of an average $\langle \bar{q} \rangle$ from this time series of column averages, (3) the collection of values of q_h at h to find an average $\langle q_h \rangle$, and (4) the calculation of $\langle \bar{W}_h \rangle$ at h , weighted by density.

Recall that the physical interpretation of Eqn. 3.3 is that a continuity relationship exists between horizontal divergence ($\bar{W}_h \bar{q}$) and subsidence at the top of the column ($\bar{W}_h q_h$) such that, if the column is to remain in steady-state over a 24-hour period, the difference between these quantities must be made up by the surface flux (S). The aircraft data served to test this steady-state assumption.

3. Linear Model to Predict PBL Concentrations (Model 1)

A preliminary flux estimation was performed using raw concentration data. However, the raw data were characterized by variations due to many factors occurring in the PBL. By limiting these factors essentially to two parameters (time

and altitude), we could capture a smoothed behavior of the column integral over the day. Furthermore, an estimate using raw data would not reflect the behavior of the forest alone; for example, local pollution from the city of Manaus could affect the concentrations of observed CO₂. Isolation of the forest uptake required identification of CO₂ anthropogenic combustion via a suitable tracer. The relatively consistent ratio of CO₂ to CO observed in pollution plumes over northeastern North America and over Amazonia (Andreae *et al.*, 1988) suggests that anthropogenic emissions of CO₂ and CO are co-located, so that CO can serve as a tracer for combustion (see Potosnak *et al.*, in press, for analysis of CO:CO₂ ratios in pollution over North America).

We used a linear model to predict concentrations of CO₂ and O₃, an approach patterned after that of Potosnak *et al.* (1999, in press). In our model (Model 1), CO₂ was determined by the predictor variables of CO (anthropogenic tracer), time, and altitude. The general equation of the linear model was:

$$[CO_2] = a_0 + a_1[CO] + \sum_{j=0}^{10} a_{2,j} \delta_{jf} \quad (3.4)$$

Here [CO₂] and [CO] denote observed concentrations, f represents time-of-day factors standing for 11 one-hour intervals (called LTF 1 – LTF 11) representing local hours 0700 to 1700, and δ is the Kronecker delta (=1 if $j = f$ and is zero otherwise). In all, 18 such models were created, each representing a 200 m altitude band. A regional background concentration of CO (CO_{background}) was determined as the 20th percentile of CO over the duration of the study. This value was inserted into Eqn 3.4 to predict concentration values of CO₂ and O₃ without the effects of anthropogenic activity. It was assumed that the flights were significantly far enough from the canopy for the forest to act as a regional sink or source.

Tables 2 and 3 display raw means and variance binned by altitude alongside relevant Model 1 regression statistics, such as r^2 and coefficients. The residual variance dramatically decreases with increasing altitude, with variance approaching a minimum of 1-2 ppm at some altitudes. Above 1500 m, the CO₂ predictions show relatively low values of r^2 (0.2-0.5); however, these do not necessarily indicate a poor fit. Because some 0.5 ppm of the variance was due solely to instrument variance as

explained in Chapter 2, low r^2 values at altitudes with low total variance partly indicate that the model could not explain the instrument variance.

A similar series of models was constructed for predicting O₃ concentrations. Unlike CO₂, the residual variance of the O₃ linear models increased with increasing altitude as concentrations increased.

3.1 Linear Model with Flight Factors (Model 2)

Flights were 3-4 hours in duration and sampled altitudes differently for the different flight objectives. To test for the possibility that variations in both CO₂ and O₃ concentrations were due mainly to flight-to-flight variation, rather than true variation with altitude and time, an additional model was constructed including factors for each flight as shown below:

$$[O_3] = a_0 + a_1[CO] + \sum_{j=0}^{10} a_{2j} \delta_{jf} + \sum_{k=0}^{13} a_{3k} \delta_{kg} \quad (3.5)$$

(The flight factors were: FLT 7, 8, 9, 11, 12, 13, 14, 15, 16, 18, 19, 20, 21, and 22, representing all the flights over the Amazon Basin with valid data for required parameters) The flight factor model for CO₂ was rejected for further analysis because the benefit gained by reducing residual variance was counteracted by the addition of numerous factors in violation of parsimony. Tables 4 and 5 compare r^2 values between Models 1 and 2 for CO₂ and O₃. The significance of the flight factors for O₃ values in flux estimation was found to be relatively minor (see Chapter 4).

3.2 Selection of h and \bar{W}

Ideal selection of h is at an altitude right above the maximum height attained by the PBL so that concentration variations and entrainment fluxes due to PBL growth do not affect the column integral. Estimation of maximum PBL height was based upon observations of concentration vertical profiles from ABLE 2B aircraft data (S.C. Wofsy, unpublished data). These data, summarized in Table 6, showed the maximum height to be about 3200m. Verification of this value was accomplished by plotting the diurnal variation of CO₂ concentrations in the altitude band 3100-3200 m in contrast to the variation within the PBL (Figure 6). However, the limited altitude

ranges of several flights (to 3100 m), prompted us to choose an alternative h at a lower altitude; thus the analysis was repeated at $h=2500$ m. As discussed in Chapter 5, choosing varying values for h offers an additional estimate of error associated with an h that is below the true maximum height of the PBL.

For $h\sim 3100$ m (~ 660 mb), a mean subsidence rate was taken to be about -600 m/day based on NCEP analyzed data from IRI/LDEO Climate Data Library (<http://ingrid.lidgo.columbia.edu>). For $h\sim 2500$ m (~ 720 mb), \overline{W}_h averaged about -550 m/day. Subsidence varied over the duration of the study period, and thus our choice of \overline{W}_h represents a temporal average for the study region. For our analysis, we accepted the assumption that -600 m/day captured most of the values of \overline{W}_h observed during the study period, $\pm\sim 50$ m/day. Issues of error associated with \overline{W} approximation are discussed in Chapter 5.

3.3 Comparison of Predicted and Raw Data

To better visualize the goodness-of-fit of Models 1 and 2, a series of flight-by-flight plots were created showing observed data of altitude, CO₂, O₃, and CO against time. Predicted values of CO₂ and O₃ were overlaid above the raw values; selected plots are shown (Figures 8 a-f). These plots show relatively close fits from both Models 1 and 2. Areas on the plots where the predicted data do not appear are due to either (1) no CO data for those observations, or (2) the observations are above 3200m, beyond which no linear models were created because of limited data at high altitudes. From these plots one also sees that the CO₂ residual variance for both models is greatest near the surface, which is explained by greater variability in the CO₂ concentrations at the surface. One can also begin to visualize the diversity of flight paths chosen during the ABLE 2B experiment.

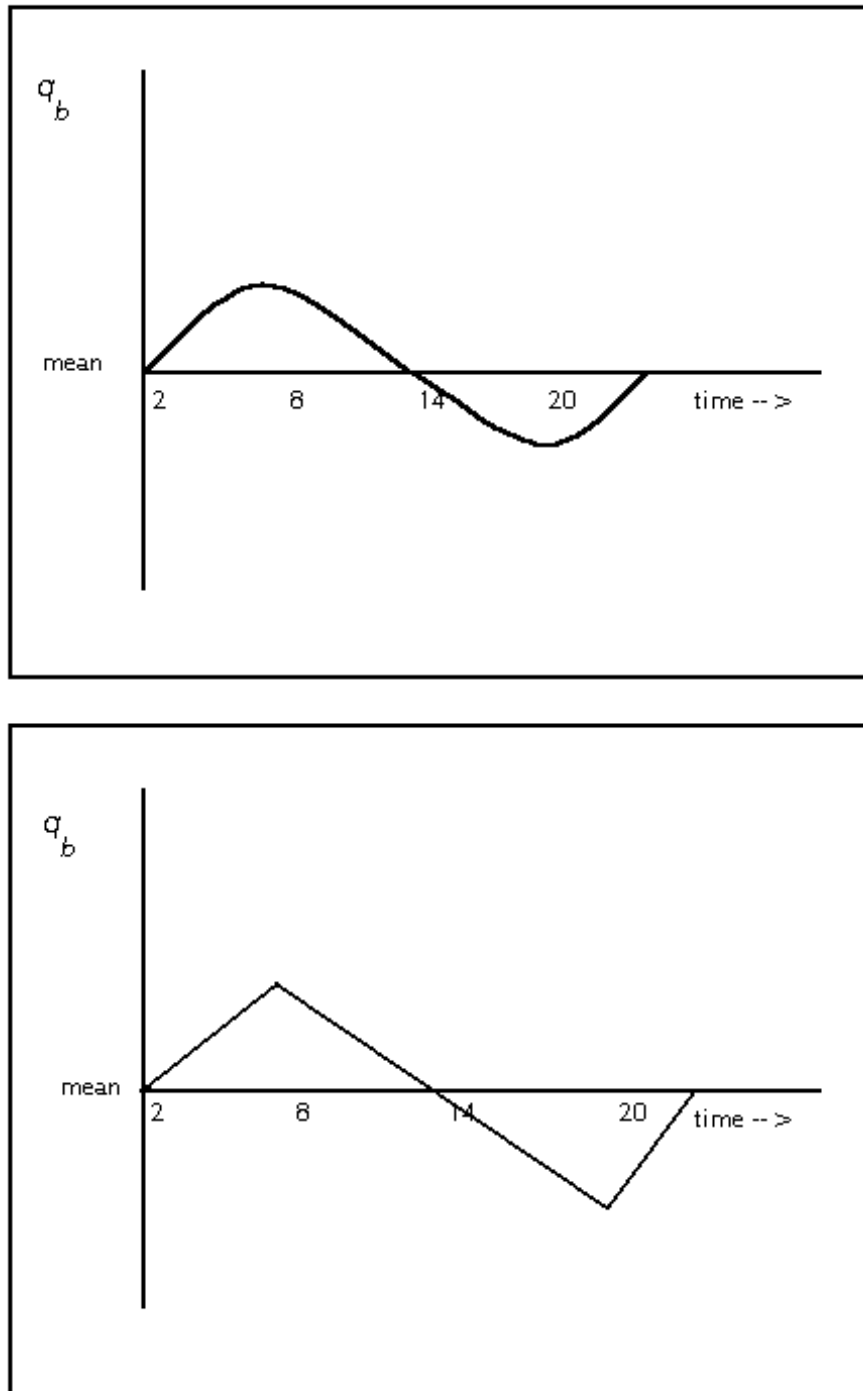


Figure 6. Two Schematics of Diurnal Variation in CO₂ Mean Column Concentration

Positive slope indicates respiration; negative slope indicates photosynthetic uptake. According to the “steady-state” assumption, the column concentration varies periodically every 24 hours. The hypothesized symmetry about the x axis signifies that the daytime mean column amount is equivalent to the 24-hour mean $\langle \bar{q} \rangle$. The “turning points” are approximately 700 and 1700 based on observations (Fan et al. 1990) of NEE response to solar flux.

$$\text{CO}_2 = a_0 + a_1[\text{CO}] + a_2\text{LTF}_i$$

Altitude (m)	Mean	Variance	R ²	Intercept	CO	LTF2	LTF3	LTF4
100	349.488	15.1119	0.7403	333.3499	0.1891	4.0150	2.3345	-2.2217
300	350.704	21.8811	0.6546	344.8028	0.0875	1.8447	2.7784	-1.0489
500	349.282	17.0268	0.5110	342.4632	0.0902	-0.3325	0.9783	1.5665
700	348.475	7.0353	0.4572	340.3419	0.0701	-0.5913	1.6857	2.4736
900	347.315	5.0563	0.4751	340.2841	0.0823	-2.2098	-1.1093	-1.8614
1100	346.738	3.0425	0.4150	340.0521	0.0667	0.0000	0.0715	-0.3281
1300	346.663	2.4562	0.3337	340.9729	0.0816	-1.7143	-1.8439	-2.0562
1500	347.107	2.5402	0.2237	341.6050	0.0692	-0.9728	-0.9269	-0.6098
1700	347.291	2.1411	0.3620	340.6511	0.0871	-1.1624	-0.7025	-0.7952
1900	347.360	1.4071	0.2432	343.6054	0.0484	-0.1524	-0.8926	-0.7087
2100	347.340	1.2413	0.3631	344.4516	0.0468	-0.6591	-1.3434	-1.3743
2300	347.391	0.9817	0.3372	344.7415	0.0371	0.0000	-0.5141	-0.6450
2500	347.449	1.2522	0.2397	343.6861	0.0516	-0.1564	-0.8008	-0.5307
2700	347.190	1.1169	0.3619	344.4262	0.0428	0.0789	-0.7595	-0.1160
2900	347.700	1.4674	0.4634	342.0612	0.0732	-0.3339	-0.3877	0.5162
3100	348.334	1.2614	0.3463	347.4970	0.0171	0.0586	-0.5567	-0.4236
3300	347.325	2.1394	0.4620	337.8054	0.1123	0.0000	-1.6952	1.2144
3500	347.350	2.8372	0.6939	334.4797	0.1569	0.0000	-2.9503	-0.1409
MEAN	347.806	5.000	0.427	341.515	0.078	-0.127	-0.369	-0.394
Altitude (m)	LTF5	LTF6	LTF7	LTF8	LTF9	LTF10	LTF11	
100	-0.5578	-2.3312	-2.8251	-7.5937	-7.9047	-7.5472	0.0000	
300	-1.7345	-3.6105	-6.1906	-7.2721	-8.5081	-10.3404	-6.8595	
500	-0.7992	-2.7439	-3.6738	-5.1336	-5.4047	-8.2522	-5.7326	
700	2.7827	2.3123	0.8383	-0.8071	-1.3685	-2.2887	-0.1460	
900	1.1346	-0.0549	0.0955	-1.8285	-2.9832	-2.3211	-1.4916	
1100	2.1406	0.3182	0.9587	-0.7654	-0.2822	-0.3308	0.0000	

$$O_3 = a_0 + a_1[CO] + a_2LTF_i$$

Altitude (m)	Mean	Variance	R ²	Intercept	CO	LTF2	LTF3	LTF4
100	9.5647	5.7452	0.4991	4.3425	0.1378	-4.5460	-7.7383	-7.7165
300	8.2463	6.0626	0.2229	11.9993	-0.0057	-3.5902	-4.7643	-4.1958
500	9.4467	4.8640	0.1544	14.7214	-0.0372	-1.2544	-2.5299	-2.8045
700	12.1081	8.4435	0.4156	7.7724	0.0466	-0.7751	-0.7437	-2.9409
900	11.7332	6.0269	0.1727	7.0810	0.0359	1.9135	2.5719	1.2729
1100	13.2465	6.9341	0.1670	7.0490	0.0725	0.0000	1.3061	-0.5523
1300	14.3656	6.3540	0.3384	9.8043	0.0589	0.6783	1.1569	0.1465
1500	15.1017	5.7710	0.3657	10.1663	0.0776	-0.1501	-0.4389	-1.7932
1700	15.7222	5.7365	0.2584	10.6658	0.0672	0.0116	0.0850	-0.4358
1900	17.0503	4.9861	0.2462	9.3699	0.0754	-0.2371	1.0031	1.8527
2100	16.7096	9.7382	0.1644	9.0070	0.0645	1.1720	2.2299	3.3052
2300	17.1151	11.8557	0.2015	10.1096	0.0901	0.0000	-0.1253	-0.3068
2500	17.8334	10.3445	0.2519	12.8751	0.0505	1.8471	1.4494	0.5543
2700	18.5788	7.7162	0.1808	23.0311	-0.0720	2.0072	3.0156	0.8976
2900	18.9267	11.7798	0.3963	35.3049	-0.2068	0.5732	2.7662	0.8767
3100	19.1500	16.1203	0.3724	39.3375	-0.2535	-0.1889	1.1260	2.0695
3300	19.0895	18.8208	0.5302	45.8644	-0.2697	0.0000	3.5899	-1.2197
3500	19.3832	17.9379	0.5649	51.0324	-0.3299	0.0000	4.2997	-3.0338
MEAN	15.187	9.180	0.306	17.752	-0.022	-0.141	0.459	-0.779
Altitude (m)	LTF5	LTF6	LTF7	LTF8	LTF9	LTF10	LTF11	
100	-8.7332	-8.3021	-8.9249	-9.1947	-8.2050	-7.9742	0.0000	
300	-1.6027	-1.4437	-3.3888	-3.4002	-2.6641	-2.3189	-3.9152	
500	-1.3317	-1.1596	-1.4888	-1.0121	-1.5914	-0.3635	-4.1223	
700	-1.7155	-1.4420	1.9301	-2.0410	-1.4504	-0.1938	-5.6028	
900	1.0109	0.4896	1.4328	-0.0684	0.6946	2.5146	-2.2565	
1100	-1.2684	-1.7021	-1.3193	-1.4705	-0.7133	-0.6242	0.0000	
1300	-0.7743	-2.1859	-1.8420	-3.4144	-1.7158	-1.6607	0.0000	
1500	-1.7988	-3.7558	-2.7158	-4.5800	-3.7798	-3.2811	0.0000	
1700	-0.9566	-0.9709	-0.9852	-3.9360	-2.6038	-1.2042	0.0000	
1900	0.8541	0.1912	1.3834	0.4381	-0.9214	-0.4774	1.6735	
2100	3.0093	1.1028	2.0374	0.6542	2.2286	0.0695	3.6377	
2300	-0.5075	-0.3757	-0.6691	-3.8944	-1.7449	-4.4223	0.8540	
2500	0.9664	2.3134	1.3299	-2.3500	-1.7089	-1.8570	1.4555	
2700	4.2906	2.3016	3.1261	-1.6796	1.5710	1.9856	0.0000	
2900	4.5188	2.9035	1.2060	-2.9911	-0.4148	1.6590	2.0871	
3100	3.6452	2.1129	5.5158	-3.5511	1.1464	1.1760	0.0000	
3300	2.3605	-1.4381	-4.0897	-8.7457	-4.7769	-2.2744	0.0000	
3500	-0.2090	-1.0040	-3.9627	-7.3032	-4.2037	-0.7953	0.0000	
MEAN	0.098	-0.687	-0.635	-3.252	-1.714	-1.113	-0.344	

Table 3. Regression Statistics for O₃ Linear Model 1

N.B. A zero value indicates the factor is not present; that time is not represented in the altitude band.

CO₂

Alt (m)	Variance	R ² (2)	R ² (1)	R ² (2) – (1)
100	21.88108	0.745766	0.654575	0.091190
300	17.02679	0.620734	0.511045	0.109689
500	7.035291	0.628014	0.457150	0.170864
700	5.056306	0.622689	0.475068	0.147621
900	3.042491	0.566308	0.415046	0.151262
1100	2.456162	0.553858	0.333668	0.220190
1300	2.540241	0.634617	0.223747	0.410870
1500	2.141106	0.718314	0.362023	0.356292
1700	1.407053	0.457054	0.243184	0.213870
1900	1.241305	0.642431	0.363148	0.279283
2100	0.981693	0.589031	0.337211	0.251820
2300	1.252202	0.533194	0.239652	0.293542
2500	1.116917	0.748859	0.361877	0.386982
2700	1.467441	0.812103	0.463450	0.348653
2900	1.261363	0.7241	0.346308	0.377792

Table 4. Comparison of r² Values: CO₂ Model 1 vs. CO₂ Model 2 (Added Flight Factors)

Model 2 shows some improvement in r² values for CO₂.

O₃

Alt (m)	Variance	R ² (2)	R ² (1)	R ² (2) – (1)
300	6.060758	0.71749	0.222859	0.494632
500	4.864046	0.733344	0.154386	0.578957
700	8.440135	0.810111	0.415551	0.394560
900	6.0269	0.763468	0.172747	0.590720
1100	6.934141	0.765258	0.167031	0.598227
1300	6.354026	0.721888	0.338362	0.383526
1500	5.770965	0.748362	0.365744	0.382618
1700	5.73651	0.7661	0.258440	0.507660
1900	4.986054	0.801112	0.246218	0.554894
2100	9.738209	0.832186	0.164404	0.667782
2300	11.85567	0.837832	0.201467	0.636365
2500	10.34446	0.860352	0.251947	0.608405
2700	7.716236	0.846634	0.180802	0.665832
2900	11.77979	0.886353	0.396289	0.490065

Table 5. Comparison of r² Values: O₃ Model 1 vs. O₃ Model 2 (Added Flight Factors)

Model 2 shows improvement in r² values for O₃.

Hour	h(t) in km
8	0.662
9	0.888
10	0.789
11	1.110
12	1.500
13	1.887
14	2.620
15	3.200
16	1.998
17	0.944

Table 6. Diurnal Variation of Boundary Layer Height

Source: S.C. Wofsy, unpublished data from ABLE 2B.

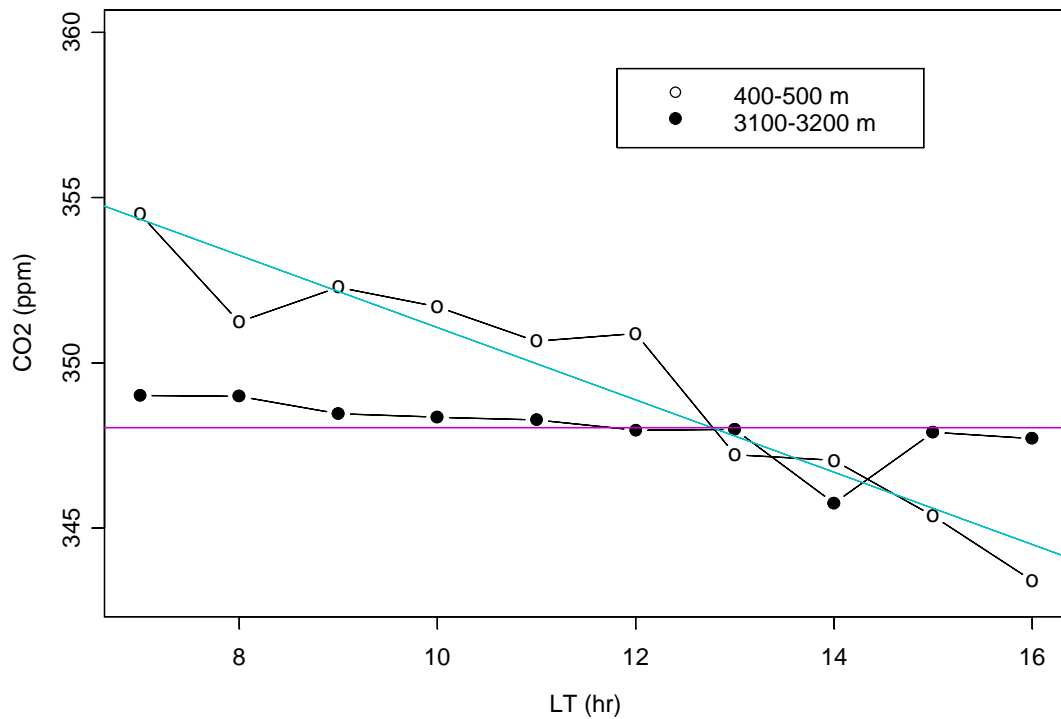


Figure 7. CO₂ Diurnal Concentration Variation Within PBL Contrasted to PBL Top

The observed concentrations at the top of the PBL (3200) are relatively stable compared to the decreasing concentrations observed at 400-500 m. N.B.: Data from raw aircraft observations alone.

Figures 8a-f. Comparison of Raw Data to Predicted Data, Models 1 (Blue) and 2 (Pink)

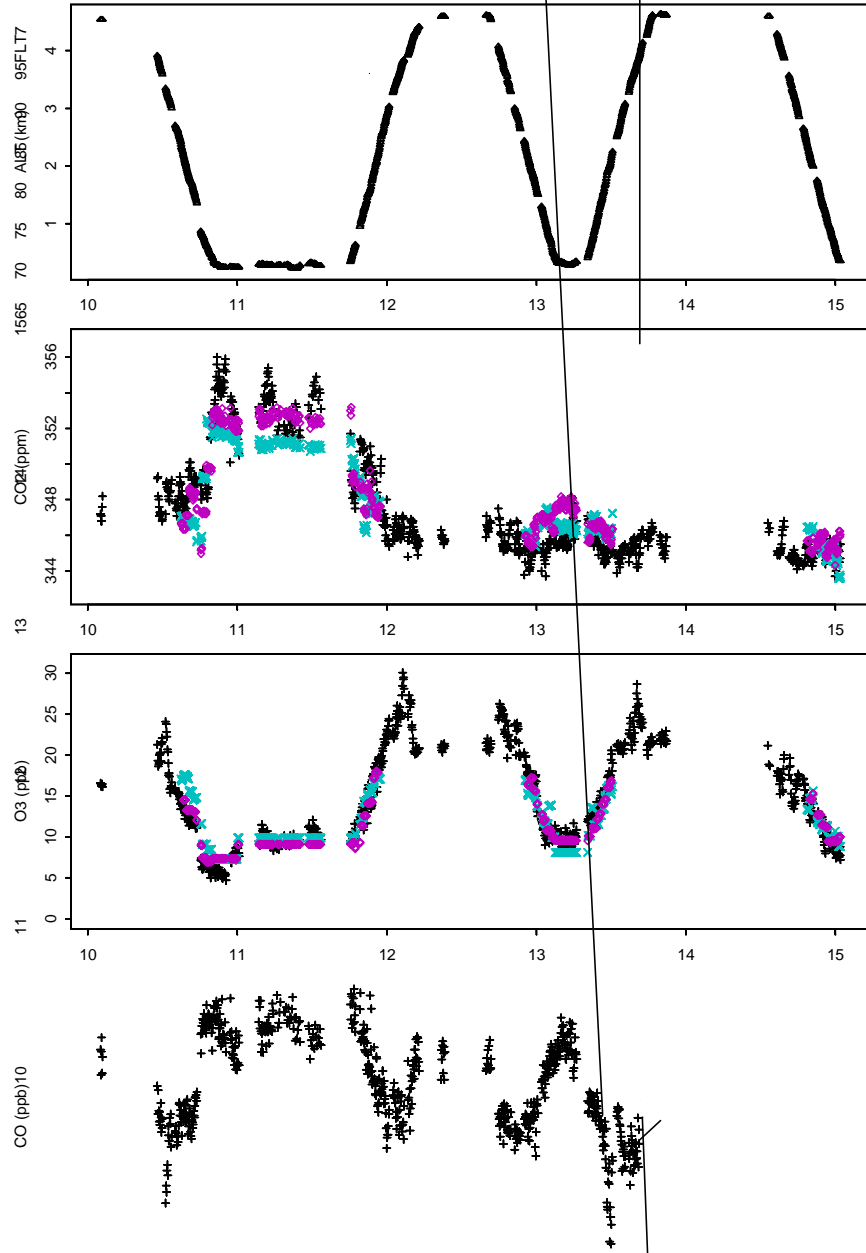


Figure 8a. Flight 7: Transport-Volume

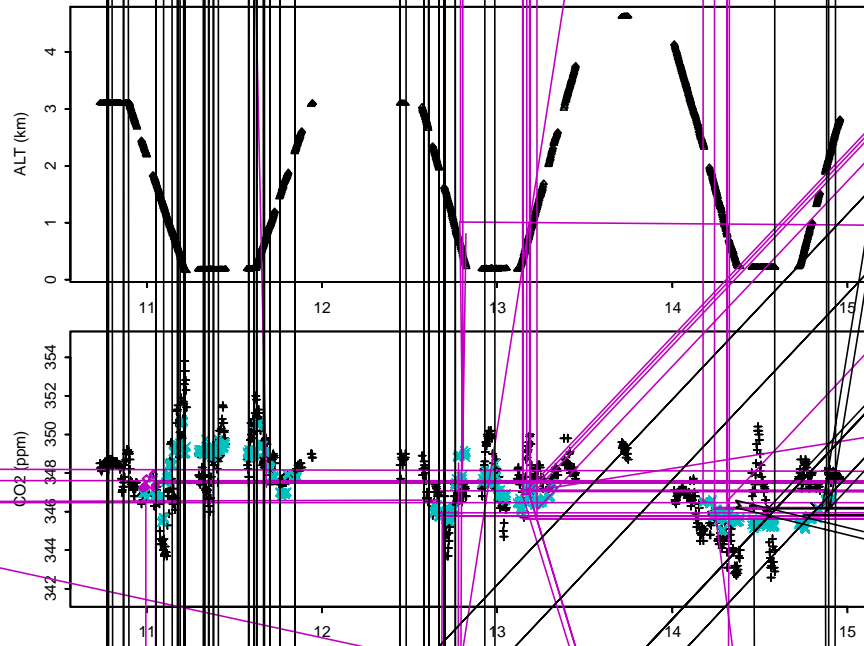
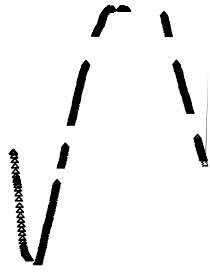


Figure 8b. Flight 8: Source
Model 1 fits in blue, Model 2 fits in pink



7

Figure 8c. Flight 9: Source
Model 1 fits in blue, Model 2 fits in pinkALT (km)

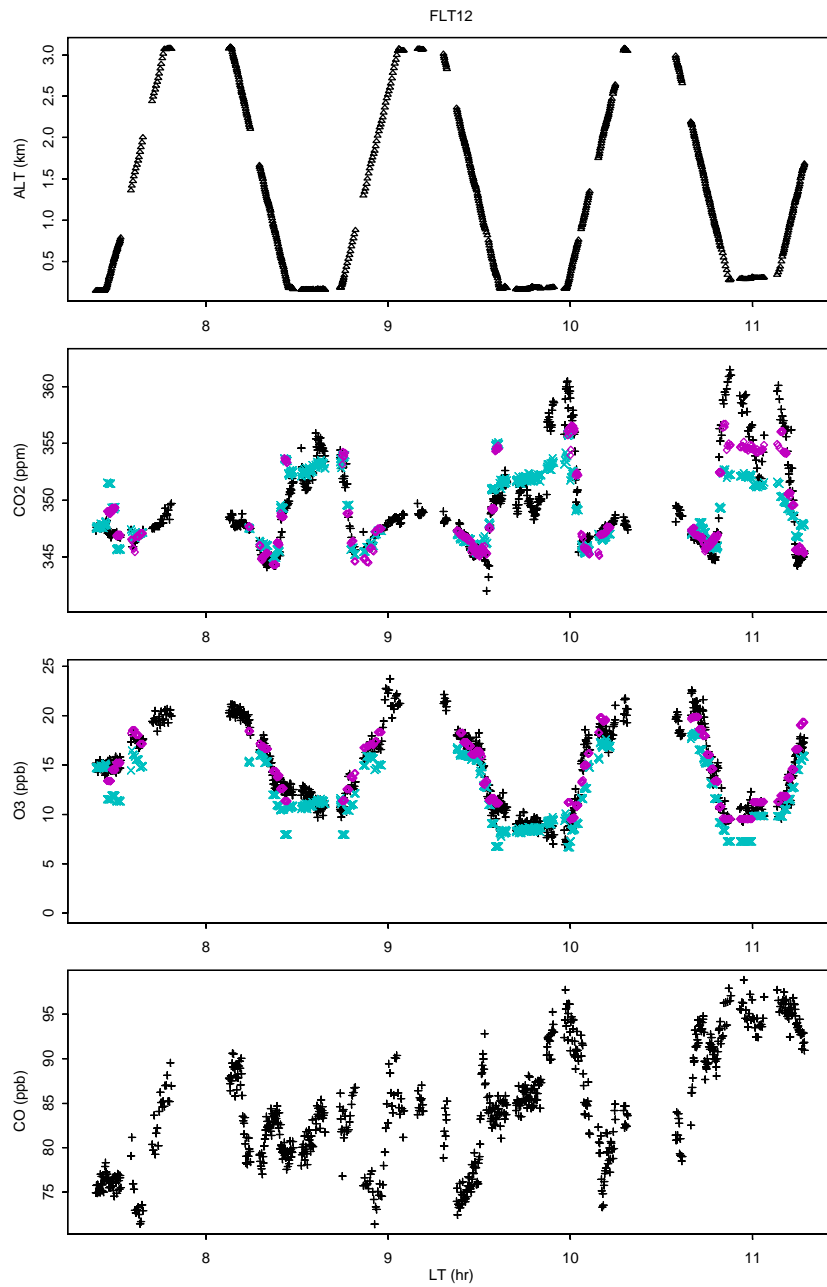


Figure 8d. Flight 12: Source
Model 1 fits in blue, Model 2 fits in pink



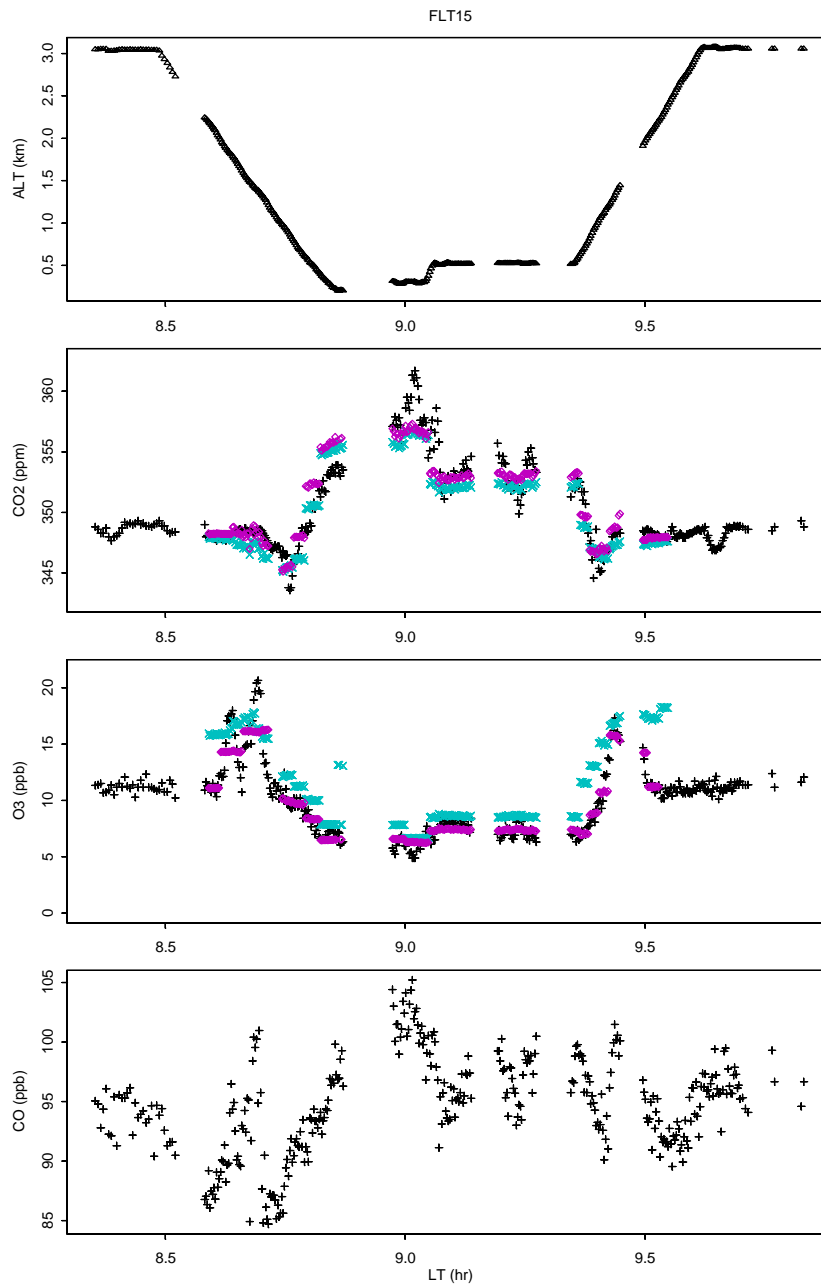


Figure 8f. Flight 15: Source
Model 1 fits in blue, Model 2 fits in pink

Chapter 4: Results

1. Observed Concentration Profiles

Daytime vertical concentration profiles were obtained for CO₂ and O₃ using only data for which CO₂ observations were available (9433 of 26965 total observations). The remaining data were checked to remove artifacts resulting from instrumentation errors. For each hour, profiles of raw CO₂ and O₃ were plotted against an altitude range of 0-5 km as a preliminary assessment of diurnal variation in CO₂ (Figures 9-10) and O₃ (Figures 11-12) concentrations. Different flights were identified by different plotting symbols. Because the altitude floor of the flights was 150 m, these aircraft vertical profiles were combined with hourly means from measurements of concentrations at 41 m (just above the canopy), the highest level of data from the eddy flux tower to provide lower boundary conditions.

The transition from stratified to mixed conditions over the day's progression is apparent from the CO₂ profiles. In the morning (0700-0900), the profiles reflect a large nocturnal build-up of CO₂ at the surface which is depleted by midday (1200) due to turbulent mixing and photosynthetic uptake. The lowest-altitude points on the profiles, representing tower data just above canopy height, one can see dramatic change over the day due to net uptake.

A positive gradient with altitude is observed in the O₃ profiles due to the effects of deposition to the surface. This gradient does not appear to have a large diurnal variation. At about 3 km, a reversal in the gradient occurs in some plots, probably due to the difference in concentrations between the PBL and the free troposphere.

2. Diurnal Trends in Aggregated Flight Data

For CO₂, daytime vertical profiles of the aggregated flight data are shown in Figure 13, further demonstrating the transition over the day from stratified to well-mixed conditions. Two types of profiles are given: predicted data generated by the linear model (Model 1); and predicted data from Model 1 with the effect of

combustion removed. The same scenarios are also displayed for O₃ (Figure 14). These plots did not include tower data.

Hourly density-weighted means of \bar{q} for both gases were found for the period 0700-1600, assuming a column height of 3200 m and including data from the eddy flux tower. Using Model 1, predicted values and predicted values minus the effects of combustion were plotted to demonstrate the daytime trend in average column concentration. These trends were: linear decrease for CO₂ (Figure 15, top panel); and fairly steady behavior for O₃ (Figure 15, bottom panel). The linear-like decrease for CO₂ over the aggregated flight data suggested that a 24-hour column steady state might be a fair approximation.

3. Estimates of CO₂ and O₃ Gradients and Fluxes

3.1 Column Integral Method (Method A)

Values of $\langle \bar{q} \rangle$ (the 24-hour average integrated concentration) for both gases were estimated by taking the mean of the PBL column amount over the daytime hours, excluding the hour of 1700 LT, during which altitude coverage in the PBL was sparse. For each gas, the altitude range of the PBL was defined in four ways, each of which yielded a different gradient magnitude. h was designated to be either 2500m or 3200 to assess the effect of unaccounted-for PBL entrainment. The minimum altitude was rounded either to 100 m (using only flight data, minimum=150m), or to 0 m (with added of data from the eddy flux tower=41m), resulting in: Case 1 (0-2500 m); Case 2 (0-3200 m); Case 3 (100-2500 m); and Case 4 (100-3200 m). From the determined values of \bar{q} and measured values of q_h at either 2600 m or 3200 m, a total of twelve $\bar{q} - q_h$ gradients were estimated for each gas, using data from raw, predicted, and predicted without combustion scenarios. These values are summarized in Tables 7 and 8. The effects that resulted from these various cases are treated in Chapter 5. The gradient using Case 2 is also shown graphically for predicted data without the effect of combustion for CO₂ (Figure 16) and O₃ (Figure 17).

Fluxes were estimated using Equation 3.3 from these gradients as well as an approximated value of \bar{W} of -600 m/day (resulting in a column replacement time of

about 1×10^6 s). The fluxes are summarized in Table 9. The best estimates are probably for Case 2: -4.8×10^{12} molecules/cm²-s for CO₂ and -6.9×10^{10} molecules/cm²-s for O₃. Inclusion or exclusion of tower data significantly affected the CO₂ flux estimation. For CO₂, removal of the combustion effect also had a very large impact, in two cases reversing the direction of the flux from positive to negative (see Chapter 5).

O₃ fluxes did not vary considerably in the four cases, leading us to conclude that depositional flux to the canopy was satisfactorily captured by the flight data, and that CO may not be well correlated with O₃. For predicted data with combustion removed, the flux was -6.9×10^{10} molecules/cm²-s.

Effect of Flight Factors

The model with flight factors (Model 2) was tested for O₃ but did not yield significantly different gradients. As Model 2 had more factors, the relative scarcity of data above 3.1 km had a greater impact on its regressions, and thus the gradient estimate was performed for an altitude of 3100 m rather than 3200 m. The predicted O₃ values with combustion removed, given by Model 2, Case 2, resulted in a $\langle \bar{q} - q_h \rangle$ gradient of (-4.3 ppb), a value similar to that generated by Model 1, (-5.6 ppb). The gradients for all model types are given in Table 8. These results suggest that flight-to-flight variation is not a major force driving gradients.

Effect of Varying \bar{W}

A change in mean subsidence, or the descent rate for air above the PBL to replace the air in the PBL, can greatly affect the CO₂ flux estimate. Figure 18 shows dramatic linear change in CO₂ flux estimate. A variation in \bar{W} of -50 m/day results in a change in the flux estimate of about 20%.

3.2 Flux Inference by Similarity (Method B)

If two tracers have similar transport characteristics, i.e. similar \bar{W} , Equation 3.3 can be rewritten for both species as:

$$\langle S_i \rangle = \langle S_j \rangle \frac{\langle q_{b;i} - q_{u;i} \rangle}{\langle q_{b;j} - q_{u;j} \rangle} \quad (4.1)$$

As a result, flux estimates can be made without requiring direct information on mean subsidence. We let species i be CO_2 and species j be O_3 . Using our knowledge of concentration gradients between the PBL and free troposphere for both tracers, we then used estimates of O_3 flux from two studies from Amazonia to perform an indirect estimate on the CO_2 flux.

Airborne measurements of O_3 flux by Ritter *et al.* (1990) during ABLE 2B gave rough bounds of -6.4 to -7.2×10^{11} molecules/cm²-s (or a mean of -6.8×10^{11}). The inferred CO_2 fluxes found using Ritter data were more than an order of magnitude larger than the fluxes estimated with the column integral method where the fluxes were derived from concentration gradients and \overline{W} (Table 10). By contrast, eddy correlation measurements by Fan *et al.* (1990), when subjected to the same similarity analysis, resulted in inferred fluxes of roughly the same order of magnitude as those found with concentration gradients and \overline{W} .

Flux inferences based on assumptions of similarity between trace gases should be viewed with caution, however, because of the uncertainties that still exist when obtaining the flux estimate for tracer j .

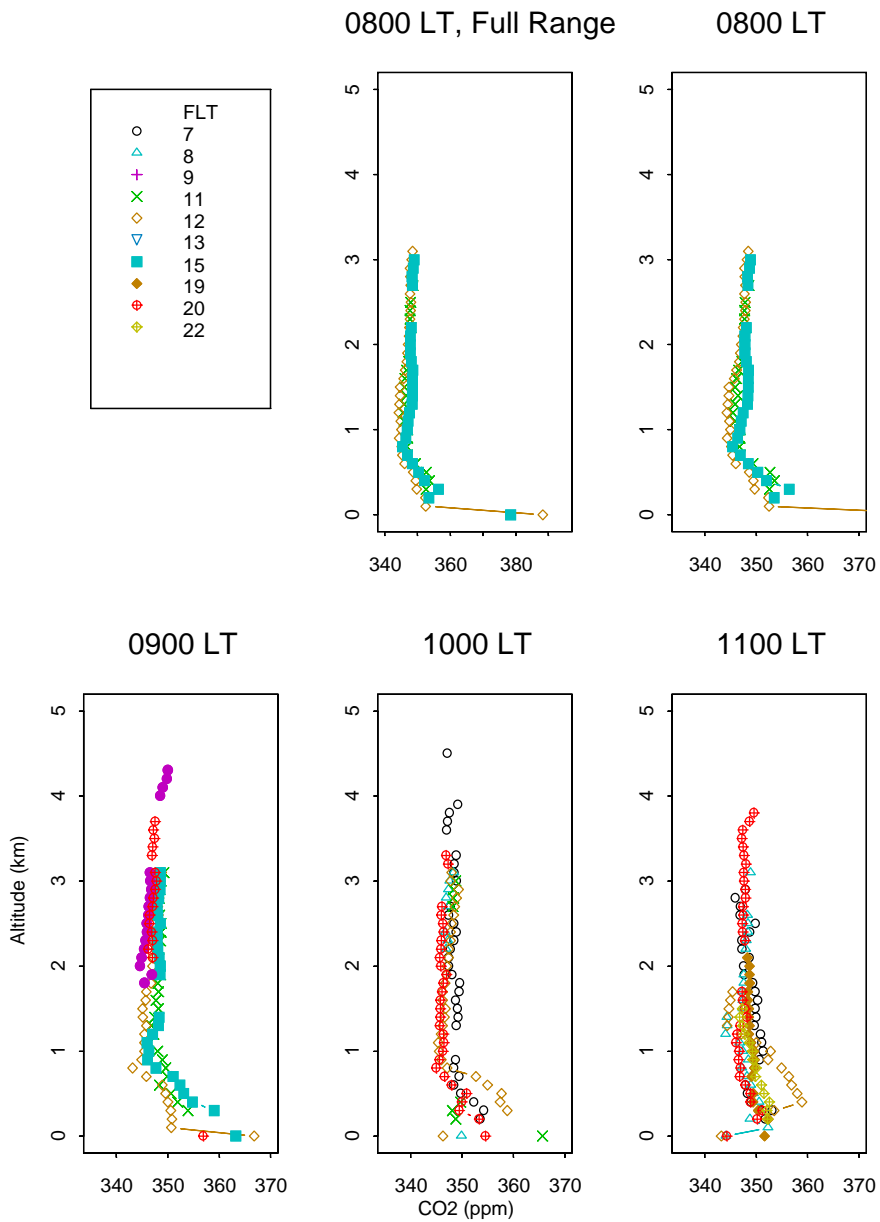


Figure 9. Hourly Plots of CO₂ Observed Profiles

The hours of 0800, 0900, 1000 Local Time (LT) show enhanced CO₂ at the surface which is eroded by midday. Each flight (FLT) has a unique plotting symbol. Tower data are not given a separate symbol but are depicted as the lowest altitude points. The first panel has a different CO₂ range than the other five because the concentrations at the surface are so high.

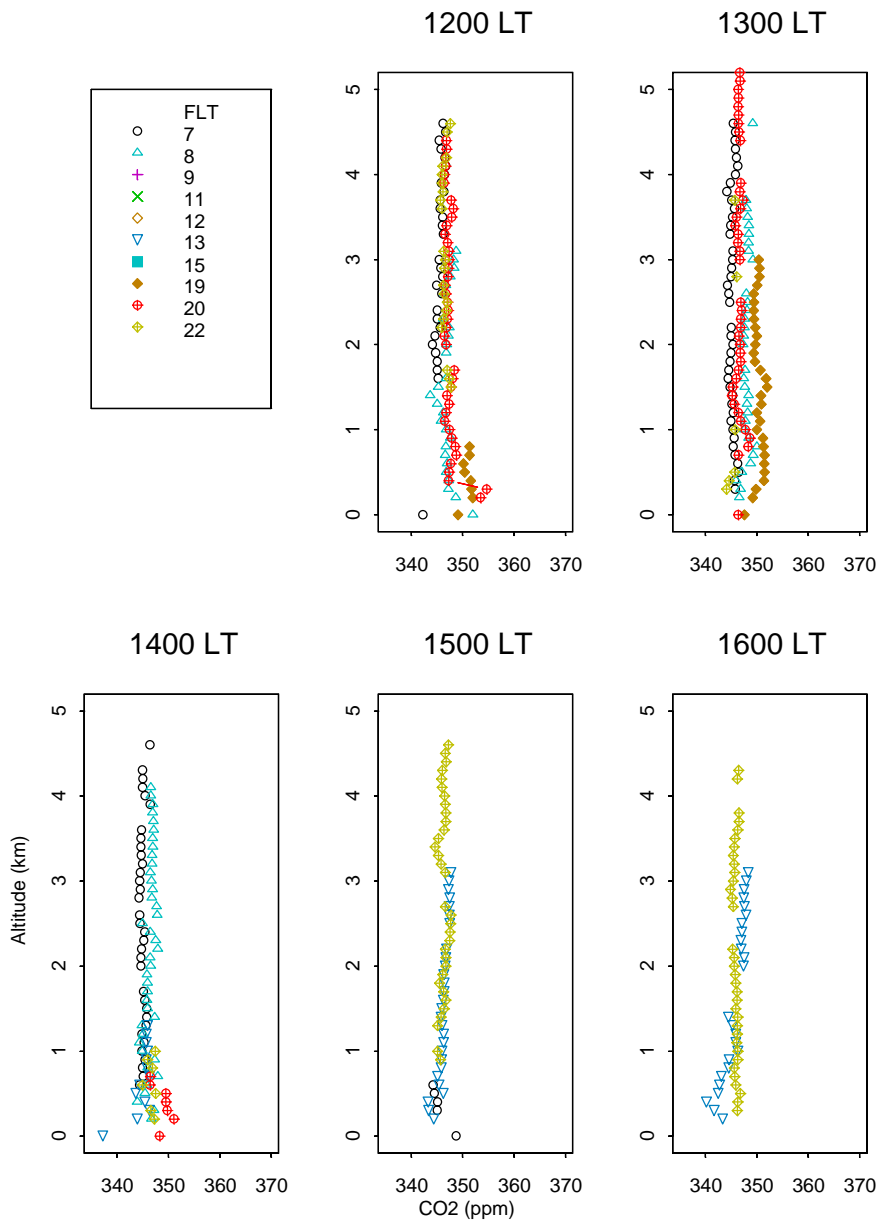


Figure 10. Hourly Plots of CO₂ Observed Profiles

The PBL is well-mixed during the afternoon.

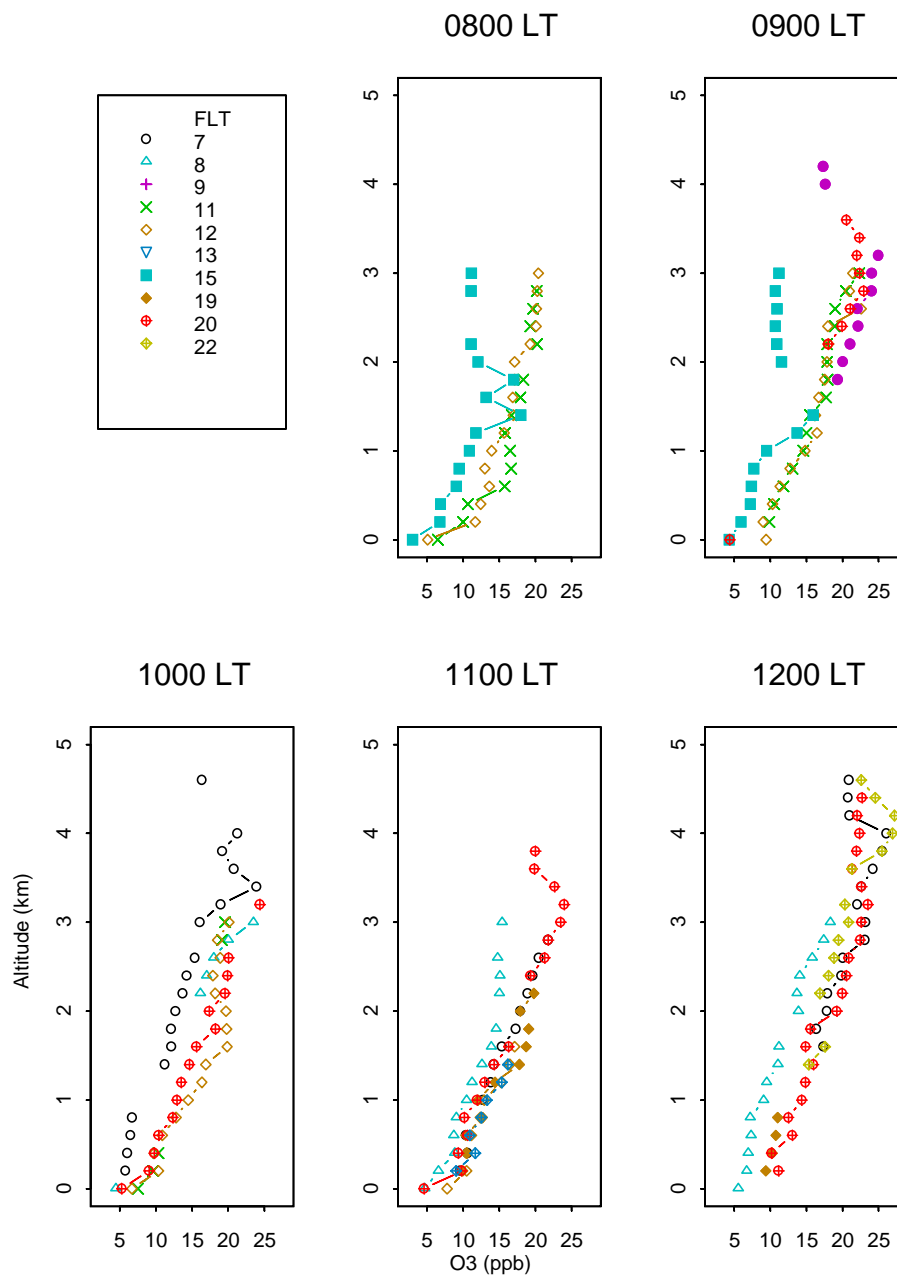


Figure 11. Hourly Plots of O₃ Observed Profiles

Gradient is fairly constant over time with lowest concentrations at the surface.

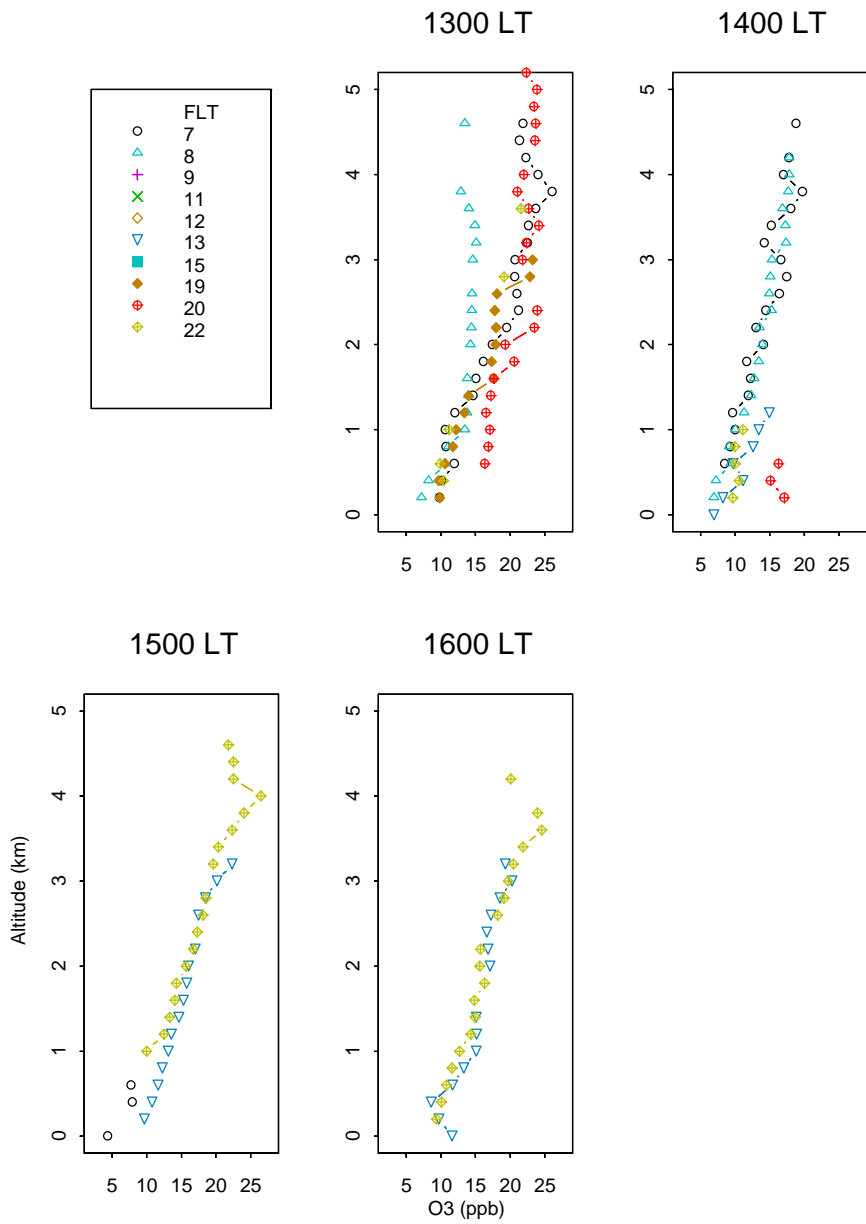
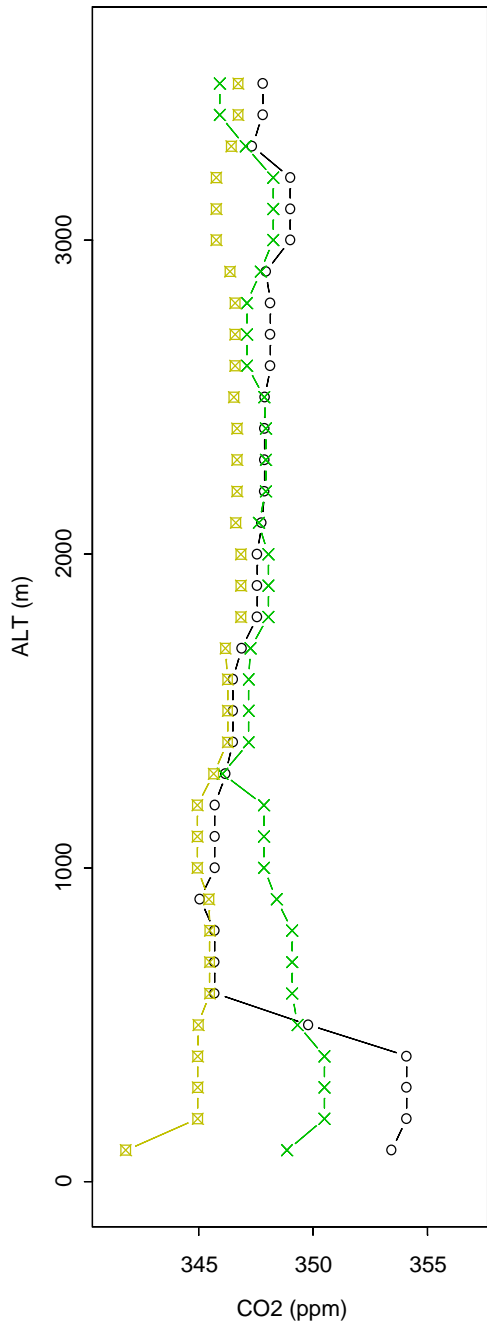
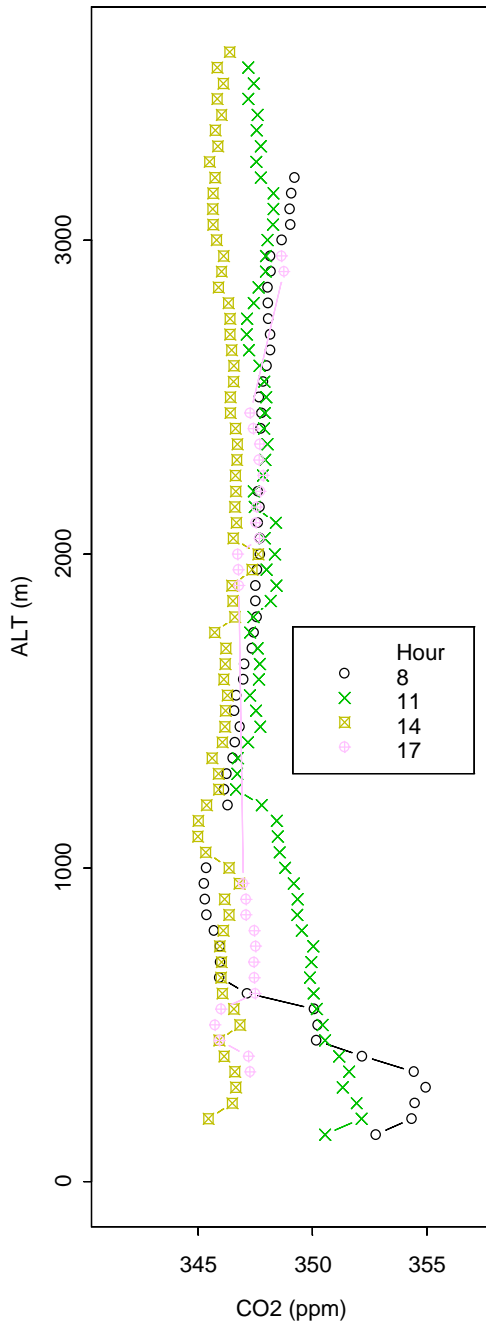


Figure 12. Hourly Plots of O₃ Observed Profiles

Predicted



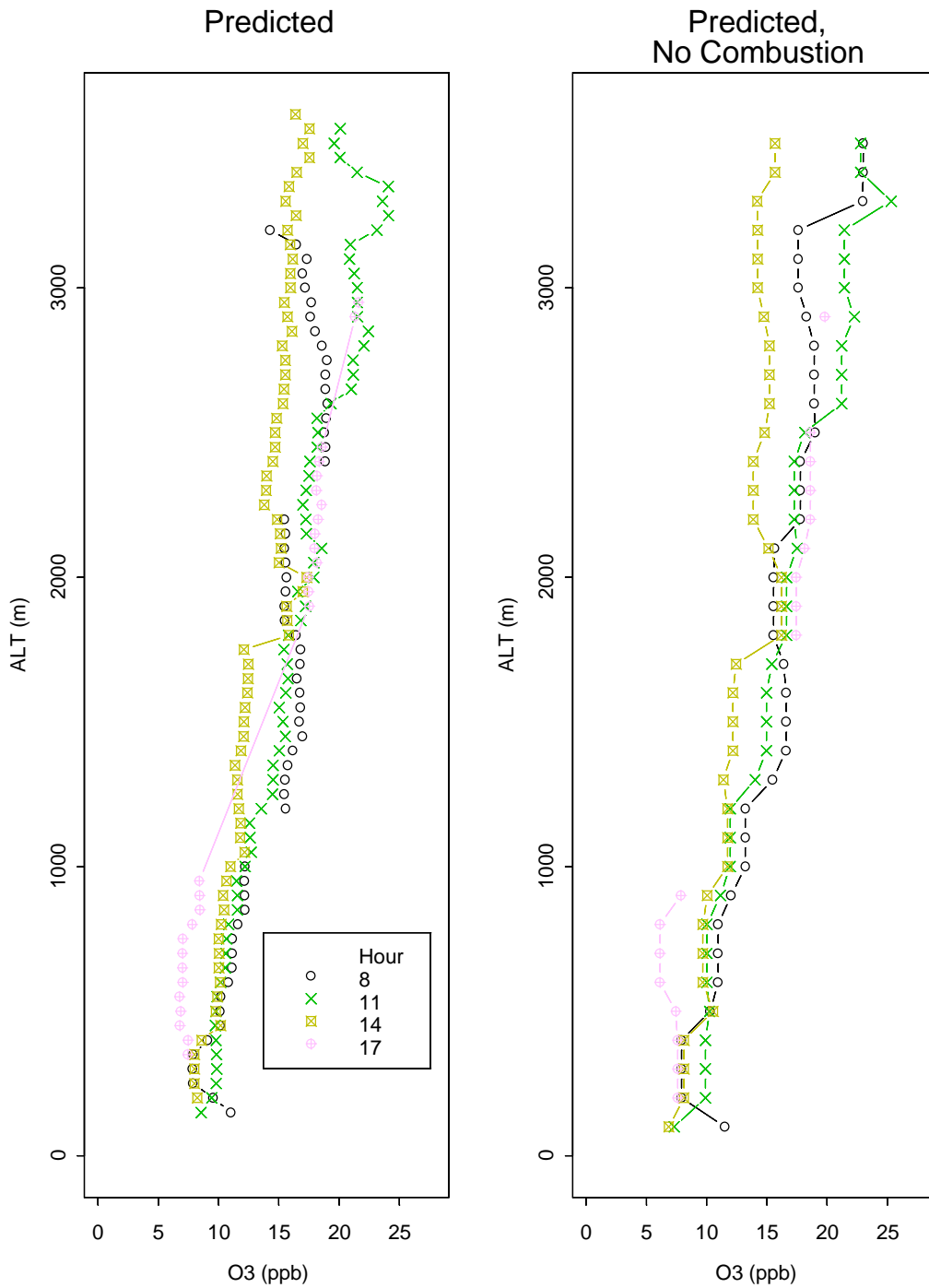


Figure 14. Vertical Profiles of Predicted O₃ From Aggregated Flight Data
O₃ concentration profile shows little diurnal variation and fairly constant altitudinal gradient.

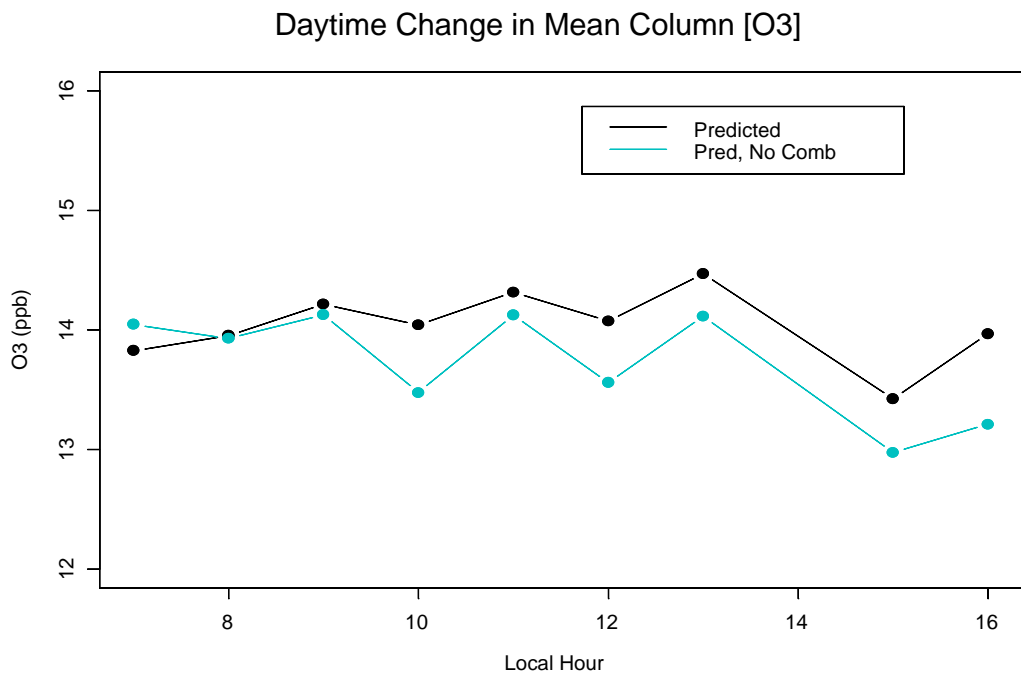
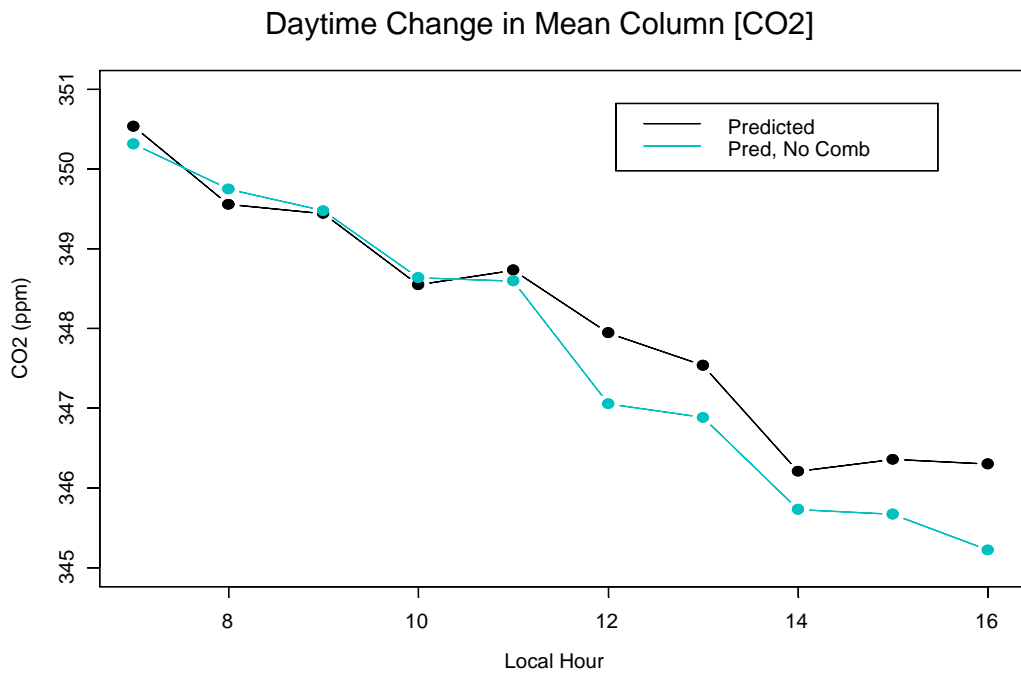


Figure 15. Diurnal Trends in Mean Column Concentration: CO₂ (upper plot) and O₃ (lower plot)

Mean column concentration for CO₂ decreased linearly; O₃ was fairly constant over the day.

N.B. The O₃ concentration at 1400 was more than 2σ below the mean and was thus omitted.

CO ₂ (ppm)			
	Raw	Predicted	Pred, No Comb
Case 1 (0-2500 m)	0.88	0.90	0.67
Case 2 (0-3200 m)	0.43	0.32	-0.39
Case 3 (100-2500 m)	0.41	0.41	-0.045
Case 4 (100-3200 m)	0.05	-0.069	-0.96

Table 7. CO₂ Daytime Gradients ($\bar{q} - q_h$)

O ₃ (ppb)					
	Model 1			Model 2	
	Raw	Predicted	Pred, No Comb	Predicted	Pred, No Comb
Case 1	-5.13	-5.27	-6.26	-6.43	-6.30
Case 2	-4.15	-4.30	-5.55	-4.77	-4.31
Case 3	-4.73	-4.87	-5.89	-6.09	-5.94
Case 4	-3.79	-3.93	-5.20	-4.45	-3.98

Table 8. O₃ Daytime Gradients ($\bar{q} - q_h$)

Model 2 gradients are not significantly different from Model 1.

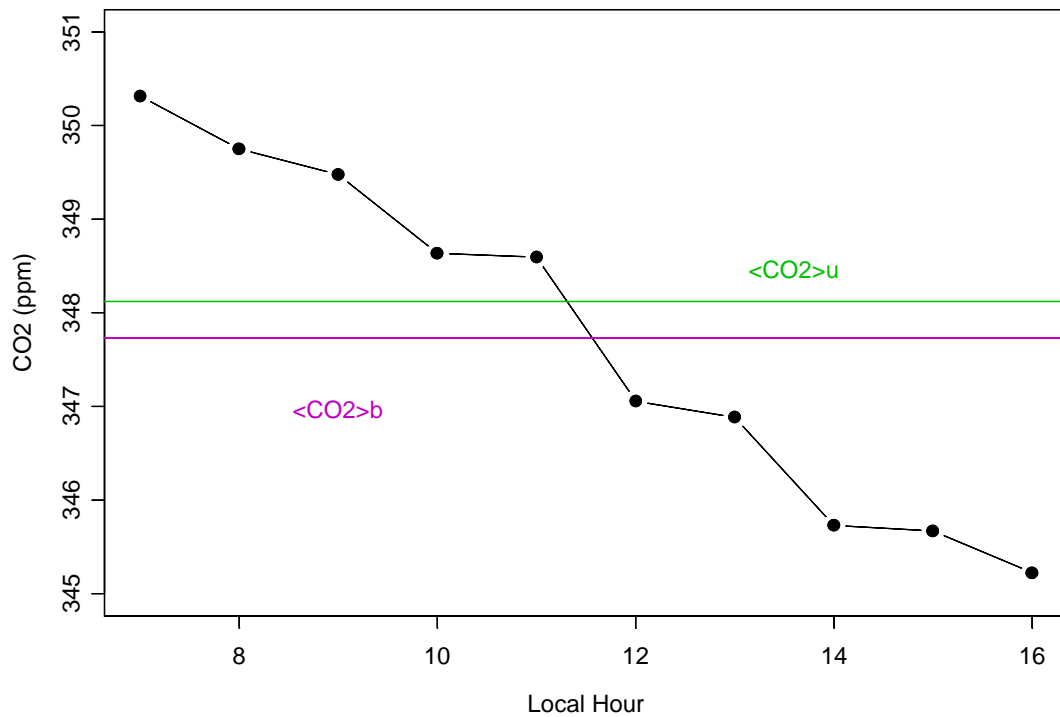


Figure 16. CO₂ Gradient $\langle \bar{q} - q_h \rangle$ for Predicted Data, Combustion Removed

The black line represents the daytime trend in column CO₂.

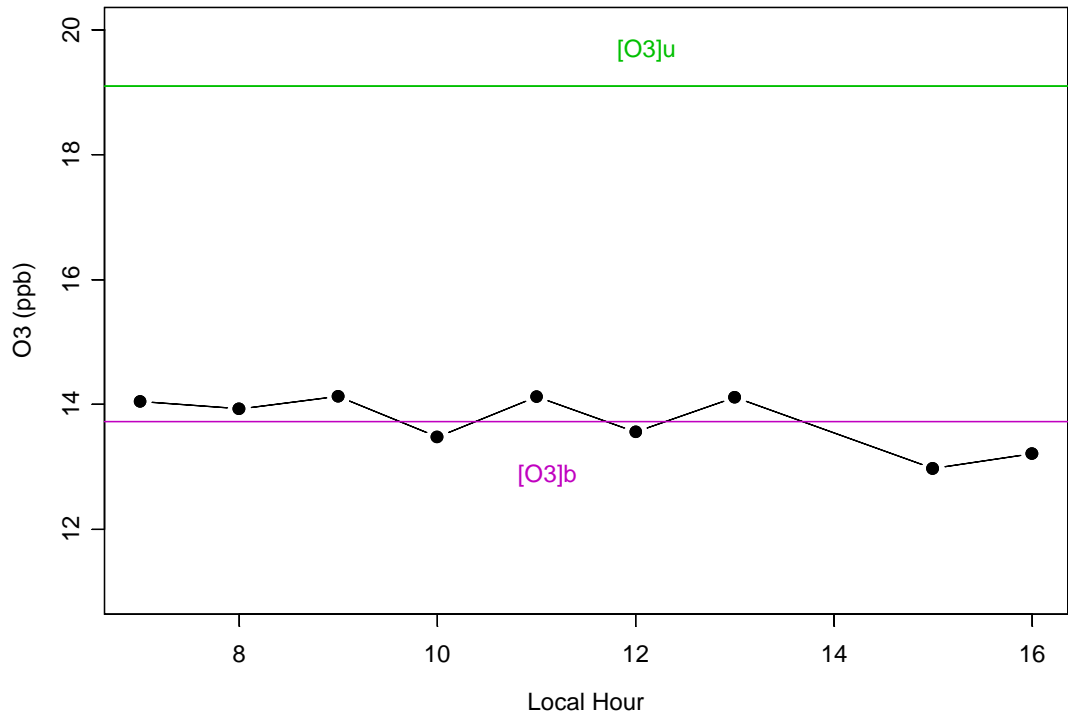


Figure 17. O₃ Gradient $\bar{q} - q_h$ for Predicted Data, Combustion Removed

The black line represents column amounts; value at 1400 was $> 2\sigma$ below the mean and was omitted.

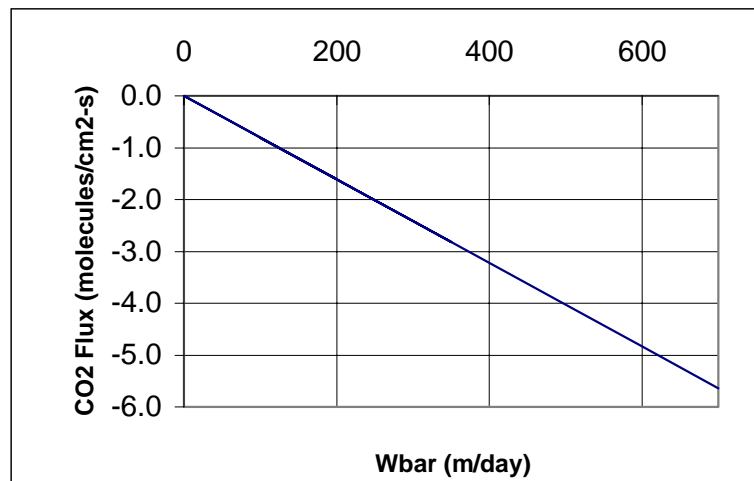


Figure 18. Dependence of CO₂ Flux on \bar{W} (using Case 2 model)

For $Wbar = -600$ m/day, the CO₂ flux is -4.83×10^{12} molecules/cm²-s (predicted data, no combustion) while for $Wbar = -650$ m/day the flux is -5.24×10^{12} molecules/cm²-s.

	Data Type	CO ₂ flux (molecules/cm ² -s)	O ₃ flux (molecules/cm ² -s)
Case 1 (0-2500 m)	Raw	1.07E+13	-6.21E+10
	Model 1	1.08E+13	-6.38E+10
	No Combustion	8.09E+12	-7.57E+10
Case 2 (0-3200 m)	Raw	5.42E+12	-5.19E+10
	Model 1	4.00E+12	-5.37E+10
	No Combustion	-4.83E+12	-6.93E+10
Case 3 (100-2500 m)	Raw	4.97E+12	-5.72E+10
	Model 1	4.96E+12	-5.89E+10
	No Combustion	-5.45E+11	-7.12E+10
Case 4 (100-3200 m)	Raw	6.62E+11	-4.73E+10
	Model 1	-8.61E+11	-4.91E+10
	No Combustion	-1.20E+13	-6.51E+10

Table 9. Summarized Flux Estimates: CO₂ and O₃

Negative values indicate loss from the atmosphere. Case 2 is of greatest interest for fullest altitude coverage. Note the sign reversals in Cases 2 and 3(for CO₂) when combustion is removed. Note that O₃ flux does not fluctuate much between scenarios.

Case	Measured or Estimated O ₃ flux	CO ₂ flux by Similarity
1	-6.4E+11*	7.3E+13
2	-6.4E+11	-4.7E+13
3	-6.4E+11	-5.2E+12
4	-6.4E+11	-1.3E+14
1	-1.0E+11 [†]	1.1E+13
2	-1.0E+11	-7.0E+12
3	-1.0E+11	-7.7E+11
4	-1.0E+11	-1.8E+13
1	-7.57E+10*	8.1E+12
2	-6.93E+10	-4.8E+12
3	-7.12E+10	-5.5E+11
4	-6.51E+10	-1.2E+13

Table 10. CO₂ Flux Estimation by Similarity

*O₃ flux data from Ritter et al. (1990)

[†]O₃ flux data from Fan et al. (1990)

*O₃ flux estimated in this study from ABLE 2B aircraft data (Method A)

All similarity calculations involved use of gradient values for the predicted data, no combustion model. All fluxes shown are in units of molecules/cm²-s. As shown in column 3, large discrepancy exists between Ritter and this study (Method A), while general agreement exists between Fan and this study.

Chapter 5: Discussion

Can the fluxes obtained in the previous chapter be reasonably extrapolated to the entire Amazon Basin over the timescale of a year? Certainly such scaling-up calculations have been attempted by other studies (Grace *et al.* 1995; Grace *et al.* 1996; Tian *et al.* 1998), but what are their limitations? A major dilemma raised by the issue of extrapolation is the amplification of systematic errors in the data collection or data analysis. Therefore, we begin our investigation of the question of extrapolation by cataloguing sources of error and bias in the ABLE 2B experiment as well as in the subsequent data analysis.

1. Sources of Error

1.1 Biases in the Data Source

The flight missions of ABLE 2B offered a comprehensive array of measurements in and above the PBL, but these data also contained biases. One problem was a systematic bias toward fair weather days due to storm-related instrument difficulties during the wet season. Fan *et al.* (1990) noted the greater tendency for the tower instrumentation to function improperly in poor weather. The relationship between CO₂ NEE and PAR (Figure 2) is such that measurements which are biased toward clear and sunny days may result in an overestimation of the forest sink. Based on available solar radiation data, Fan *et al.* (1990) calculated a 90 W/m² difference between the solar flux during the entire study period and the intervals of flux data collection. To correct for the fair weather bias, they reduced their estimates of CO₂ uptake from -0.93 kg C/ha-h to -0.25 kg C/ha-h. (Fan *et al.* 1990)

Were solar flux data for the aircraft missions available, estimates could be made as to the magnitude of the bias. Incident solar radiation data were originally acquired at the EMBRAPA station using an analog sensor. These data were digitized, but over time became irretrievable and the original charts were likewise unrecoverable. (S.C. Wofsy, personal communication, 1999).

1.2 Statistical and Systematic Error in the Data Analysis

From the methods described in Chapter 3, we know that our measurement of flux depends on the proper calculation of the concentration gradient $\langle \bar{q} - q_h \rangle$ and the choice of \bar{W} . As shown in Table 9 (Chapter 4), estimation of $\langle \bar{q} - q_h \rangle$ was affected by three adjustable factors: estimation of h , inclusion or exclusion of tower data, and removal of combustion. The influences of these factors on the gradient estimate are summarized in the next section. In addition, statistical error implicit in the $\langle \bar{q} - q_h \rangle$ gradient calculations came from two sources: prediction of concentrations by the linear model, and calculation of column integrals. Other uncertainty in the analysis framework includes the supposition that the entire daytime range between turning points was covered during the study (see Chapter 3, Figure 6).

1.3 Factors Affecting $\langle \bar{q} - q_h \rangle$ Gradient Estimation

If h is chosen to be lower than the actual top of the PBL, the PBL grows beyond h and the region above the defined column undergoes vertical mixing in and out of the column. Values of \bar{q} and q_h will thus be additionally influenced by entrainment rather than only subsidence (W) and biotic exchange (NEE). In particular, q_h may be overestimated because it will be affected by higher concentrations within the PBL. The results for CO₂ in Table 9 showed that for all model types (Raw; Predicted; Predicted, No Combustion), a choice of $h = 3200$ m instead of 2500 m resulted in $\langle \bar{q} - q_h \rangle$ gradients that were more negative. The gradient *changes* ranged from -0.4 ppm to -1.1 ppm, with an average change of -0.6 ppm. By contrast, raising h to 3200 m caused positive gradient changes for O₃ ranging from 0.7 ppb to 1.0 ppb. The implications affect our assessment at $h = 3200$ as well. If the PBL grew beyond 3200 m, we could be underestimating the actual CO₂ gradient and overestimating the O₃ gradient.

Uncertainty in lower boundary conditions (0-100 m) was indicated by the changes in gradient when tower data were included or excluded from the gradient calculations. Inclusion of CO₂ tower data always caused positive changes in gradient due to the enhanced concentrations nearer to the surface during the daytime from the

diurnal rectifier effect as shown in Chapter 4, Figures 9-10. O₃ tower data, with low surface concentrations, caused the gradient to be more negative (recall Chapter 4, Figures 11-12). The gradient changes ranged from 0.5 to 0.7 ppm (CO₂) and from -0.37 to -0.4 ppb (O₃).

Removal of combustion via the linear model caused negative changes in $\langle \bar{q} - q_h \rangle$ for both CO₂ and O₃, ranging from -0.2 to -0.9 ppm (CO₂) and -1.0 to -1.3 ppb (O₃). This reflected the contribution of anthropogenic combustion in elevating boundary layer CO₂ and O₃ concentrations.

Statistical Error

Linear model statistics were presented in Chapter 3. However, one additional error source regarding the model CO coefficients was the identification of CO as correlated solely with anthropogenic combustion. In fact, natural sources of CO, such as the oxidation of biogenic hydrocarbons, do exist. Assessment of the magnitude of this error would require measurement of biogenic hydrocarbons in the field, information unavailable from the ABLE 2B flight data.

The average column integral for a particular hour was estimated from aggregated flight data for which observations were more concentrated at low altitudes, especially 200-300 m and 300-400 m (see Table 11 for sample sizes over hours 7-17 and altitudes 100-3200 m) Without the tower data, the 100 m altitude bin was sparsely covered due to the minimum aircraft flight level of 150 m, highlighting the importance of filling in these gaps with tower observations.

Table 11 also indicates a scarcity of data during the hours of 0700 and 1700. This raises questions about how accurately our observations characterized column amounts at the turning points of the diurnal column concentration curve. However, the linear decrease in the CO₂ column amount seems to demonstrate a high degree of predictability over the period 0700-1600 (Figure 15, Chapter 4), a confirmation of the expected paradigm discussed in Chapter 3. This feature is a promising indication that estimation of the daytime average will be closely approximated by our daytime range, even if the endpoints are imperfectly defined.

Error from \overline{W} Estimation

While the sign of the concentration gradient determines the direction of the flux due to subsidence, \overline{W} only changes the magnitude of this flux, and is thus a multiplicative, not additive, error. \overline{W} is known to increase with increasing altitude and also varies according to meteorological conditions. From NCEP analysis data available at Lamont-Doherty Earth Observatory (<http://ingrid.ldgo.columbia.edu>), we found that the mean subsidence over Amazonia measured at ~660 mb was -600 m/day, although Garstang *et al.* (1990) found \overline{W} for the PAM (Portable Automated Mesonet) four-tower network to be -375 m/day over the month of the study period. However, their measurement occurred at a height just above the canopy, ~0.5 km (~950 mb), a much lower altitude, and therefore was not applicable for estimation of $\overline{W}_{z=h}$. If a smaller mean subsidence such as -375 m/day truly had existed, the magnitude of our flux would be decreased by about 40% in the case of CO₂ (Figure 18). However, because this error is multiplicative, it is not a primary source of concern.

2. Extrapolation of Results to the Basin Scale

Case 2 (where combustion was removed and $h = 3200$) was chosen for extrapolation because it contained nearly complete data coverage over the day. Our flux estimate for CO₂ of -4.8×10^{12} molecules/cm²-s was equivalent to a daily ecosystem exchange of -0.83 kg C/ha-day (1 hectare=10⁴m²) or about -0.3 tons C/ha-yr. This represents a small net exchange that, if multiplied by the size of the entire basin, would scale up to only -0.15 Gt C/yr.

2.1 Summary of Other Estimates From the Field

The eddy correlation measurements from towers and aircraft in the Amazon provide useful comparison with our results.

Eddy Flux Towers

As noted in the previous section, Fan *et al.* (1990) found a 24-hour mean NEE of -0.25 kg C/ha-h or -6.0 kg C/ha-day (Fan *et al.*, 1990). Our value for daily NEE

was much lower, -0.83 kg C/ha-day. This can probably be explained by the dense forest of the tower site and inoperability of the equipment during inclement weather, contrasted to the Electra missions which flew over wetlands and river regions and also sampled during showery periods, although not in heavy rain.

In their eddy correlation measurements in Rondônia (10°S, 57°W), Grace *et al.* (1996) reported an annual mean NEE of 8.5 mol C/m²-yr (which equals -2.79 kg C/day) and 1.0 ton C/ha-yr. The gradient $\langle \bar{q} - q_h \rangle$ associated with Grace's flux (1.62x10¹³ molecules/cm²-s) was estimated with Equation 3.3, assuming $\bar{W} = -600$ m/day. The resulting gradient of 1.3 ppm was greater than that which was observed in ABLE 2B data (<1 ppm).

Problems with the analysis of Grace *et al.* may relate to issues of nighttime respiration during stable conditions associated with low windspeed, which make these observations difficult in tall vegetation. An underestimation of nighttime efflux due to low windspeed would signify an overestimate of net uptake. It is unfortunate that our measurements made in an earlier decade cannot define current conditions, but it is encouraging that the fluxes inferred by Grace *et al.* could be detected from aircraft if they pertained to a large region.

Eddy Correlation Onboard Aircraft

The O₃ flux reported by Ritter, -6.4 to -7.2x10¹¹ molecules/cm²-s O₃, appears too negative to be supported by a typical deposition velocity over the region (~0.5-1.0 cm/s), given the low ambient concentrations in the region (0-20 ppb). The corresponding CO₂ flux by similarity would be on the order of magnitude 1x10¹⁴ molecules/cm²-s. By our estimations, this flux would have necessitated a huge $\langle \bar{q} - q_h \rangle$ gradient of ~8 ppm. Ritter *et al.* (1990) were the first to conduct airborne eddy correlation measurements over tropical forest, so comparison to similar experiments could not be drawn. However, we note that their O₃ flux measurements were much larger than those observed by Fan *et al.* (1990) on the tower over the same time period.

2.2 Spatial and Temporal Variability

Some of the discrepancy between estimates by this study, Fan, and Grace may in fact be resolved by landscape heterogeneity and interannual variability.

Importance of Vegetation Type

Wetlands and riparian regions clearly do not have the same rates of uptake as *cerrado*, woodland savanna vegetation, or forest vegetation. Spatial variability as modeled by Tian *et al.* (1998) showed how carbon exchange was positive in some regions of the Amazon and negative elsewhere. O₃ deposition, too, depends on the type of vegetation; in temperate forest O₃ deposition velocity ranges from 0-1.0 cm/day (Munger *et al.* 1996), yet in tropical forest, deposition velocities upwards of 2.0 cm/day have been observed due to the lush vegetation (Fan *et al.*, 1990). The ABLE 2B missions included flight paths over rivers and wetlands, which is one possible explanation of the smaller uptake.

Importance of Interannual Climate Variability

Tian *et al.* (1998) calculated the Amazon to be a small net source of CO₂ (+0.2 Gt C) during 1987, the year of the ABLE 2B experiment. Their results, based on a model which accounted for variations in temperature, precipitation, and other climate factors, suggest that large interannual variation in NEE could be due to influence from El Niño-Southern Oscillation (ENSO) events. By contrast, the net flux during 1989, a La Niña year, was estimated to be -0.3 Gt C, showing the Amazon to be a net sink (Tian *et al.* 1998). Interestingly, over the entire period 1980-1994, which experienced frequent ENSO episodes, Tian *et al.* (1998) found that the Amazon region took up an average net 0.2 Gt C per year.

According to available meteorological data (Garstang *et al.* 1990), 200.3 mm of rainfall fell during the month of April 1987. From the data Riebeiro *et al.* (1981) for 16 years of rainfall, the total rainfall during ABLE 2B was about 112 mm below the mean. As Tian *et al.* suggest, this water stress may have affected NEE during 1987.

3. Implications for Future Experiment Improvement

Analysis of the ABLE 2B data identified certain areas of improvement for future studies on trace gas fluxes.

Lower Boundary Conditions

This analysis showed that the inclusion of tower data at 41 m had a significant effect on the flux estimate, suggesting that future studies involving aircraft data must incorporate adequate measurements below the lowest altitude of the aircraft. An example of an extremely useful data source might be the 400 m tall tower erected by Bakwin *et al.* and other similar towers (Bakwin 1995).

Combustion and CO Oxidation

The impact on flux estimates caused by removing the effects of combustion supports the increased use of simultaneous measurements of anthropogenic tracers such as CO. In fact, additional tracers of anthropogenic activity might also be considered, such as C¹⁴, acetylene (C₂H₂) or sulfur hexafluoride (SF₆), for comparison with CO.

Measurement of isoprene, the most abundant biogenic hydrocarbon, should be included to help define biogenic CO:CO₂ ratios and to better determine their significance. The role of isoprene and other biogenic trace gases may have been underestimated in non-temperate regions (Keller *et al.* 1999). Information on isoprene would also improve O₃ chemistry modeling.

4. Conclusions

The study region was determined to be a net sink for both CO₂ and for O₃, though the mean column concentrations of the two gases behaved very differently over the day. CO₂ uptake by the forest was fairly constant over the during the day, as seen by the linear drop in column concentration. The steady nature of column O₃ over the day, however, was consistent with the covariance of surface reactivity (i.e. stomatal opening) and turbulent transport: O₃ is deposited during the day and preserved at night. By contrast, CO₂ is taken up by day and produced at night, producing a diurnal pattern of much larger fluctuation.

The CO₂ fluxes found with this method are lower than those found with eddy correlation studies, and roughly comparable to the small fluxes computed in the modeling study of Tian *et al.* Variation between the study results may be partly explained through temporal and spatial variability, or may also be due to error. Our estimates fall within the bounds of other studies, with the implication that the net flux during the ABLE 2B period was quite small. With the basin-scale extrapolation the total ecosystem uptake is between 0.1 and 0.2 Gt C/yr.

The column integral method is a valid analysis technique which, despite uncertainties, allows us to make quantitative estimates of the fluxes over a region. This method is conceptually elegant but logistically challenging due to the wide range of altitudes and times that must be sampled. Ideally we would increase the number of flights, extend the sampling time ranges, and supplement the flight data with measurements between 0-150 m on tall towers. Keeping these factors in mind, the column integral method can be a very powerful analysis tool capable of estimating regional net fluxes.

Hour/Alt (m)	100	200	300	400	500	600	700	800	900	1000	1100	1200	1300	1400	1500	1600
7	18	6	10	11	13	11	12	12	4	1	NA	NA	2	5	5	6
8	3	88	38	22	21	23	21	37	19	15	17	15	20	17	14	18
9	1	179	125	21	82	20	23	18	21	20	24	20	20	19	17	12
10	NA	125	185	102	22	19	18	16	15	13	17	10	14	11	10	10
11	4	250	115	24	24	24	23	22	21	26	24	23	23	19	22	22
12	19	109	67	119	19	19	100	37	16	14	14	14	13	12	14	14
13	NA	38	132	20	26	14	23	182	50	28	20	20	23	17	23	23
14	NA	166	212	40	75	37	18	20	28	53	10	8	16	13	10	9
15	NA	31	30	16	15	14	11	8	10	28	8	5	8	11	9	10
16	NA	68	34	12	11	12	11	14	17	18	15	14	16	10	12	12
17	NA	NA	1	6	4	3	3	4	6	NA	NA	NA	NA	NA	NA	NA
Hour/Alt	1700	1800	1900	2000	2100	2200	2300	2400	2500	2600	2700	2800	2900	3000	3100	3200
7	7	6	5	5	NA	NA	NA	1	6	7	6	6	6	22	8	NA
8	15	14	14	10	18	22	17	17	15	7	12	26	10	64	29	4
9	12	16	29	18	21	28	26	21	19	24	22	28	27	35	56	NA
10	15	15	13	16	14	19	14	14	12	13	13	12	13	22	69	8
11	18	14	5	5	49	5	9	8	10	12	6	6	5	4	7	4
12	8	5	10	13	17	15	14	12	12	17	16	17	20	22	26	7
13	23	14	17	51	15	14	11	9	11	7	4	28	10	39	12	12
14	10	3	7	119	9	9	12	12	13	13	7	7	7	7	6	7
15	18	12	14	8	8	5	1	2	7	10	66	12	8	37	16	5
16	13	11	10	17	14	10	8	8	8	11	14	18	17	81	24	12
17	NA	NA	2	2	3	4	5	4	NA	NA	NA	NA	3	NA	NA	NA

Table 11. Table showing sample sizes used in the column integral procedure.

Data is concentrated at altitudes of 200 and 300 m. Data is relatively scarce for altitude bands at 100 and 3200 m. The hours of 7 and especially 17 have relatively sparse data.

References

- Anderson, B. E., Gregory, G. L., Collins, J. E., Sachse, G. W., Conway, T. J., and Whiting, G. P. (1996). "Airborne observations of spatial and temporal variability of tropospheric carbon dioxide." *Journal of Geophysical Research*, 101(D1), 1985-1997.
- Andreae, M. O., Browell, E. V., Garstang, M., Gregory, G. L., Harriss, R. C., Hill, G. F., Jacob, D.J., Pereira, M. C., Sachse, G. W., Setzer, A. W., Dias, P. L. S., Talbot, R. W., Torres, A. L., and Wofsy, S. C. (1988). "Biomass-burning emissions and associated haze layers over Amazonia." *J. Geophys. Res.*, 93(D2), 1509-1527.
- Bakwin, P. S., Tans, P. P., Zhao, C., William Ussler, I., and Quesnell, E. (1995). "Measurements of carbon dioxide on a very tall tower." *Tellus*, 47B, 535-549.
- Brown, S., and Schroeder, P. E. (1999). "Spatial patterns of aboveground production and mortality of woody biomass based on inventory data for eastern U.S. forests." *Ecological Applications*, in press.
- Brown, S., Schroeder, P., and Birdsey, R. (1997). "Aboveground biomass distribution of US eastern hardwood forests and the use of large trees as an indicator of forest development." *Forest Ecology and Management*, 96(1-2), 37-47.
- Ciais, P., Tans, P. P., Trolier, M., White, J. W. C., and Francey, R. J. (1995). "A large northern hemisphere terrestrial CO₂ sink indicated by the ¹³C/¹²C ratio of atmospheric CO₂." *Science*, 269, 1098-1102.
- Conway, T. J., Tans, P. P., Waterman, L. S., Thoning, K. W., Kitzis, D. R., Masarie, K. A., and Zhang, N. (1994). "Evidence for interannual variability of the carbon cycle from the National Oceanic and Atmospheric Administration/Climate Monitoring and Diagnostics Laboratory Global Air Sampling Network." *Journal of Geophysical Research*, 99(D11), 22831-22855.
- Denmead, O. T., Raupach, M. R., Dunin, F. X., Cleugh, H. A., and Leuning, R. (1996). "Boundary layer budgets for regional estimates of scalar fluxes." *Global Change Biology*, 2, 255-264.
- Denning, A. S., Fung, I. Y., and Randall, D. (1995). "Latitudinal gradient of atmospheric CO₂ due to seasonal exchange with land biota." *Nature*, 376, 240-243.
- Denning, A. S., Randall, D. A., Collatz, G. J., and Sellers, P. J. (1996). "Simulations of terrestrial carbon metabolism and atmospheric CO₂ in a general circulation model. Part 2: Simulated CO₂ concentrations." *Tellus*, 48B, 543-567.
- Enting, I. G., Trudinger, C. M., and Francey, R. J. (1995). "A synthesis inversion of the concentration and delta-C-13 of atmospheric CO₂." *Tellus*, 47B(1-2), 35-52.
- Fan, S., Gloor, M., Mahlman, J., Pacala, S., Sarmiento, J., Takahashi, T., and Tans, P. (1998). "A large terrestrial carbon sink in North America implied by atmospheric and oceanic carbon dioxide data and models." *Science*, 282, 442-446.
- Fan, S.-M., Wofsy, S. C., Bakwin, P. S., and Jacob, D. J. (1990). "Atmosphere-biosphere exchange of CO₂ and O₃ in the central Amazon forest." *Journal of Geophysical Research*, 95(D10), 16851-16864.
- Garstang, M., Ulanski, S., Greco, S., Scala, J., Swap, R., Fitzjarrald, D., Martin, D., Browell, E., Shipman, M., Connors, V., Harriss, R., and Talbot, R. (1990). "The Amazon Boundary-Layer Experiment (ABLE 2B): A meteorological perspective." *Bulletin American Meteorological Society*, 71(1), 19-32.

- Grace, J., Lloyd, J., McIntyre, J., Miranda, A., Meir, P., Miranda, H., Moncrieff, J., Massheder, J., Wright, I., and Gash, J. (1995). "Fluxes of carbon dioxide and water vapor over an undisturbed tropical forest in south-west Amazonia." *Global Change Biology*, 1(1), 1-12.
- Grace, J., Lloyd, J., McIntyre, J., Miranda, A. C., Meir, P., and Miranda, H. S. (1996a). "Carbon dioxide flux over Amazonian rain forest in Rondonia." Amazonian deforestation and climate, J. H. C. Gash, C. A. Nobre, J. M. Roberts, and R. L. Victoria, eds., John Wiley & Sons, Chichester, 307-318.
- Grace, J., Malhi, Y., Lloyd, J., McIntyre, J., Miranda, A. c., Meir, P., and Miranda, H. S. (1996b). "The use of eddy covariance to infer the net carbon dioxide uptake of Brazilian rain forest." *Global Change Biology*, 2, 209-217.
- Gregory, G. L., Browell, E. V., and Warren, L. S. (1990). "Amazon basin ozone and aerosol: wet season observations." *J. Geophys. Res.*, 95(D10), 16903-16912.
- Harriss, R. C., Garstang, M., Wofsy, S. C., Beck, S. M., Bendura, R. J., Coelho, J. R. B., Drewry, J. W., J.M. Hoell, Jr., Matson, P. A., McNeal, R. J., Molion, L. C. B., Navarro, R. L., Rabine, V., and Snell, R. L. (1990a). "The Amazon Boundary Layer Experiment: Wet Season 1987." *J. Geophys. Res.*, 95(D5), 16721-16736.
- Harriss, R. C., Sachse, G. W., Hill, G. F., Wade, L. O., and Gregory, G. L. (1990b). "Carbon monoxide over the Amazon Basin during the wet season." *J. Geophys. Res.*, 95(D10), 16927-16932.
- Harriss, R. C., Wofsy, S. C., Garstang, M., Browell, E. V., Molion, L. C. B., McNeal, R. J., J.M. Hoell, J., Bendura, R. J., Beck, S. M., Navarro, R. L., Riley, J. T., and Snell, R. L. (1988). "The Amazon Boundary Layer Experiment (ABLE 2A): Dry Season 1985." *J. Geophys. Res.*, 93(D2), 1351-1360.
- IPCC. (1995). *Climate Change 1994: Radiative Forcing of Climate Change*, Cambridge University Press, Cambridge.
- Jacob, D. J., and Wofsy, S. C. (1990). "Budgets of reactive nitrogen, hydrocarbons, and ozone over the Amazon Forest during the wet season." *J. Geophys. Res.*, 95(D10), 16737-16754.
- Keller, M., and Lerdau, M. (1999). "Isoprene emission from tropical forest canopy leaves." *Global Biogeochemical Cycles*, 13(1), 19-29.
- McNeal, R. J. (1988). "Global Tropospheric Experiment Chemical Instrumentation Test And Evaluation Results (GTE ABLE-2A) - Preface." *J Geophys Res*, 93(D2), 1349.
- Munger, J. W., Wofsy, S. C., Bakwin, P. S., Fan, S.-M., Goulden, M. L., Daube, B. C., Goldstein, A., Moore, K. E., and Fitzjarrald, D. R. (1996). "Atmospheric deposition of reactive nitrogen oxides and ozone in a temperate deciduous forest and a subarctic woodland 1. Measurements and mechanisms." *Journal of Geophysical Research*, 101(D7), 12639-12657.
- Phillips, O. L., Malhi, Y., Higuchi, N., Laurance, W. F., Nunez, P. V., Vasquez, R. M., Laurance, S. G., Ferreira, L. V., Stern, M., Brown, S., and Grace, J. (1998). "Changes in the carbon balance of tropical forests: evidence from long-term plots." *Science*, 282, 439-442.
- Potosnak, M. J., Wofsy, S. C., Denning, A. S., Conway, T. J., and Barnes, D. H. "Influence of biotic exchange and combustion on atmospheric CO₂ concentrations in New England from observations at a forest flux tower." *J. Geophys. Res.* (in press).
- Prentice, I. C., and Lloyd, J. (1998). "C-quest in the Amazon Basin." *Nature*, 396, 619-620.

- Raupach, M. R., Denmead, O. T., and Dunin, F. X. (1992). "Challenges in linking atmospheric CO₂ concentrations to fluxes at local and regional scales." *Australian J. of Botany*, 40(4-5), 697-716.
- Riebeiro M., de O. M., A. Filho, dos Santos H. M., and dos Santos, J. M. (1981). "Estudos climatológicos da Reserva Florestal Ducke-Manaus-AM." *Acta Amazonica*, 11, 759-768.
- Ritter, J. A., Lenschow, D. H., Barrick, J. D. W., Gregory, G. L., Sachse, G. W., Hill, G. F., and Woerner, M. A. (1990). "Airborne flux measurements and budget estimates of trace species over the Amazon basin during the GTE/ABLE 2B expedition." *J. Geophys. Res.*, 95(D10), 16875-16886.
- Sandermann, H., Wellburn, A. R., and Heath, R. L. (1997). *Forest Decline and Ozone*. Ecological Studies, Springer-Verlag, Berlin, 398.
- Santos, J. (1987). "Climate, natural vegetation and soils in Amazonia: an overview." *The Geophysiology of Amazonia: Vegetation and Climate Interactions*, R. Dickinson, ed., Wiley-Intersciences, New York, 25-36.
- Schimel, D. S. (1995). "Terrestrial Ecosystems and the Carbon-Cycle." *Global Change Biology*, 1, 77-91.
- Schroeder, P., S. Brown, J.M. Mo, R. Birdsey, and C. Cieszewski (1997). "Biomass estimation for temperate broadleaf forests of the United States using inventory data." *Forest Science*, 42(3), 424-434.
- Shuttleworth, W. J., Gash, J. H. C., Lloyd, C. R., Moore, C. J., Roberts, J., Filho, A. D. O. M., Fisch, G., Filho, V. D. P. S., Ribeiro, M. D. N. G., Molion, L. C. B., Sa, L. D. D. A., Nobre, J. C. A., Cabral, O. M. R., Patel, S. R., and Moraes, J. C. D. (1984). "Eddy correlation measurements of energy partition for Amazonian forest." *Quart. J. R. Met. Soc.*, 110, 1143-1162.
- Stephens, B. B., S.C. Wofsy, R.F. Keeling, and P. P. Tans (1998). "The CO₂ Budget Rectification Airborne Study." submitted to *AGU Geophysical Monograph on Inverse Methods in Global Geochemical Cycles*.
- Stull, R. B. (1988). *An Introduction to Boundary Layer Meteorology*, Kluwer Academic Publishers, Dordrecht.
- Tans, P. P., I. Y. Fung, and T. Takashi (1990). "Observational constraints on the global atmospheric CO₂ budget." *Science*, 247, 1431-1438.
- Tian, H. Q., Melillo, J. M., Kicklighter, D. W., McGuire, A. D., Helfrich, J. V. K., Moore, B., and Vorosmarty, C. J. (1998). "Effect of interannual climate variability on carbon storage in Amazonian ecosystems." *Nature*, 396, 664-667.
- Turner, D., Koerper, G., Harmon, M., and Lee, J. (1995). "A carbon budget for forests of the conterminous United States." *Ecological Applications*, 5(2), 421-436.
- Vachalek, R. E., Stull, R. B., and Eloranta, E. W. (1988). "Mean vertical velocity and divergence measurements in the boundary layer." *J. Appl. Meteor.*
- Wofsy, S. C., Harriss, R. C., and Kaplan, W. A. (1988). "Carbon dioxide in the atmosphere over the Amazon basin." *J. Geophys. Res.*, 93(D2), 1377-1387.

Appendix I

(source: Steven C. Wofsy, personal communication)

Continuity equation and layer budget CO₂ over a forest

The continuity equation is given by

$$\frac{\partial n_q}{\partial t} + \nabla \cdot \Phi_q = 0 \quad (1)$$

where $\Phi = (u\hat{i} + v\hat{j} + w\hat{k})n_q = \mathbf{V}n_q$, and we note that $\nabla \cdot n\mathbf{V} = -\partial n/\partial t = 0$, for n the number density of air (mass continuity equation).

We now substitute for the mole fraction (mixing ratio) q , $n_q = n(z)q(z)$, to get

$$n(z) \frac{\partial q}{\partial t} + \nabla \cdot \mathbf{V}q n(z) = 0. \quad (2)$$

We integrate over the volume with height h , taken to be the altitude of the highest level reached by the PBL during the day, i.e. integrate by $\frac{1}{h} \int_0^h dz \int_0^{\Delta x} dx \int_0^{\Delta y} dy \dots$.

The first term gives $\frac{1}{h} \frac{\partial}{\partial t} \int_0^h n(z)q(z;t) dz = \frac{1}{h} \frac{\partial q_b}{\partial t} \times \int_0^h n(z) dz$, where we have assumed that q_b is independent of x and y at each altitude and $q_b = \int_0^h n(z)q(z;t) dz / \int_0^h n(z) dz$. This assumption makes the various averages over x and y equal and neglects horizontal advection terms (e.g. $\frac{\partial n_q}{\partial x}$) and time dependence of $n(z)$.

The second term is, by the divergence theorem,

$$\frac{1}{h} \int_0^h dz \int_0^{\Delta x} dx \int_0^{\Delta y} dy \nabla \cdot \mathbf{V}q n = \frac{1}{h} \int_S \hat{\mathbf{n}} q n dS$$

where S is the surface of the integration volume and $\hat{\mathbf{n}}$ is the normal to the surface. The integrals over the six sides of the rectangular solid are thus

$$\begin{aligned} & \frac{1}{h} \int_0^{\Delta x} dx \int_0^{\Delta y} dy [(wqn)_{z=h} - (wqn)_{z=0}] + \frac{1}{h} \int_0^h dz \int_0^{\Delta y} dy [(uqn)_{\Delta x=x} - (uqn)_{0=x}] \\ & + \frac{1}{h} \int_0^h dz \int_0^{\Delta x} dx [(vqn)_{\Delta y=y} - (vqn)_{0=y}] \end{aligned}$$

The first term becomes $\frac{1}{h} \left[\bar{W}_{z=h} q(z=h) n(z=h) - \hat{S} \right]$, where $\bar{W}_{z=h}$ is the mean subsidence rate at $z = h$ and \hat{S} is net ecosystem exchange (carried by turbulent motions, since $\bar{W}_{z=0} = 0$). The differences in the last two terms can be evaluated using a Taylor series expansion,

$$(uqn)_{\Delta x=x} = (uqn)_{0=x} + \frac{\partial}{\partial x} [(uqn)]_{x=0} \Delta x,$$

to give

$$0 = \frac{1}{h} \left[\bar{W}_h q_h n_h - \hat{S} \right] + \frac{1}{h} \int_0^h dz q n \left[\frac{\partial u}{\partial x} + \frac{\partial v}{\partial y} \right] \quad (3)$$

and applying the mass continuity equation,

$$0 = \frac{1}{h} \left[\bar{W}_h q_h n_h - \hat{S} \right] - \frac{1}{h} \int_0^h dz q \frac{\partial n w}{\partial z}.$$

If we assume that $\nabla_h \cdot \mathbf{V}n = \text{constant}$, then

$$\frac{\partial n w}{\partial z} = C_1$$

or $nw = C_1 z + C_2$. Applying the boundary conditions for \bar{W} ,

$$\bar{W}(0) = 0 \text{ and } \bar{W}(h) = \bar{W}_h \Rightarrow C_2 = 0 \text{ and } C_1 = \bar{W}_h n_h / h$$

to give the final form of the equation,

$$\frac{\partial q_h}{\partial t} + \left[\bar{W}_h q_h n_h - \hat{S} \right] - \bar{W}_h n_h \bar{q} = 0, \quad (4)$$

where $\bar{q} = \frac{1}{h} \int_0^h q(z;t) dz$. If we assume that $q(z;t)$ is periodic (i.e. $q(z;t) = q(z;t + T)$, $T=24$ hrs), and average equation (4) over 24 hours ($\frac{1}{T} \int_0^T dt \dots = \langle \dots \rangle$), we obtain

$$\bar{W}_h n_h \left[q_h - \langle \bar{q} \rangle \right] = \hat{S}. \quad (5)$$

This is the equation solved for the ABLE-2B data set.

Note that there is an alternative view of a tropical boundary layer under suppressed conditions, such that subsidence $\bar{W}_h n_h$ is balanced by convection that carries mass from the PBL to altitudes above h . In the extreme case where all the subsidence flux was balanced in this way, the budget equation averaged over 24 hours becomes

$$\bar{W}_h n_h \left[q_h - \langle q_{PBL} \rangle \right] = \hat{S}. \quad (5')$$

If we use the mass-weighted mean $\int_0^h n(z)q(z)dz / \int_0^h n(z)dz$ in place of \bar{q} , or Eq. (5'), we obtain slightly different budget equations to compare to the results of Eq. (5).